The Contribution of Host Galaxy Properties in X-Ray Active Galactic Nuclei Clusters

Gutu Dereje Mekonen

A Thesis Submitted to the Department of Applied Physics,

School of Applied and Natural Science

Presented in Partial Fulfillment of the Requirement for the Degree of Master's in Astrophysics (M.Sc. in Astrophysics)

Office of Graduate Studies

Adama Science and Technology University

June, 2023

Adama, Ethiopia

The Contribution of Host Galaxy Properties in X-Ray Active Galactic Nuclei Clusters

Gutu Dereje Mekonen

Advisor: Anno Kare (PhD)

Co-advisor: Megersa Wodajo (PhD)

A Thesis Submitted to the Department of Applied Physics,

School of Applied and Natural Science

Presented in Partial Fulfillment of the Requirement for the Degree of Master's in Astrophysics (M.Sc. in Astrophysics)

Office of Graduate Studies

Adama Science and Technology University

June, 2023

Adama, Ethiopia

DECLARATION

I hereby declare that this Master Thesis entitled "**The Contribution of Host Galaxy Properties in X-Ray Active Galactic Nuclei Clusters**" is my original work. That is, it has not been submitted for the award of any academic degree, diploma or certificate in any other university. All sources of materials that are used for this thesis have been duly acknowledged through citation.

______________________________ ______________________ ____________________

Name of the student Signature Date

RECOMMENDATION

We, the advisors of this thesis, hereby certify that we have read the revised version of the thesis entitled "**The Contribution of Host Galaxy Properties in X-Ray Active Galactic Nuclei Clusters**" prepared under our guidance by Gutu Dereje submitted in partial fulfillment of the requirements for the degree of Masters of Science in Astrophysics. Therefore, we recommend the submission of revised version of the thesis to the department following the applicable procedures.

______________________	______________________	______________________
Major Advisor	Signature	Date
______________________	______________________	______________________
Co-advisor	Signature	Date

APPROVAL SHEET

We, the advisors of the thesis entitled "**The Contribution of Host Galaxy Properties in X-Ray Active Galactic Nuclei Clusters**" and developed by Gutu Dereje, hereby certify that the recommendation and suggestions made by the board of examiners are appropriately incorporated into the final version of the thesis.

Major Advisor Signature Date

Co-advisor Signature Date

We, the undersigned, members of the Board of Examiners of the thesis by Gutu Dereje have read and evaluated the thesis entitled "**The Contribution of Host Galaxy Properties in X-Ray Active Galactic Nuclei Clusters"** and examined the candidate during open defense. This is, therefore, to certify that the thesis is accepted for partial fulfillment of the requirement of the degree of Master of Science in Astrophysics.

Chairperson Signature Date

Internal Examiner Signature Date

External Examiner Signature Date

Final approval and acceptance of the thesis is contingent upon submission of its final copy to the Office of Postgraduate Studies (OPGS) through the Department Graduate Council (DGC) and School Graduate Committee (SGC).

Department Head Signature Date

School Dean Signature Date

Office of Postgraduate Studies, Dean Signature Date

ACKNOWLEDGEMENT

First and foremost, I want to thank "**Almighty GOD**" for blessing me with good health and providing me the opportunity to undertake this thesis. Next, I would like to extend my deepest thanks to my advisor and instructor, Dr. Anno Kare. I am incredibly grateful for his consistent guidance, valuable suggestions, and assistance throughout this research work. His expertise, mentorship, and dedication have been instrumental in shaping the direction of this thesis. I am grateful for his unwavering support, sharing of skills and experiences, and the meaningful relationship we have built. Furthermore, I express my heartfelt appreciation to Dr. Megersa Wodajo, my co-advisor, for his valuable time, insightful feedback, and contribution to this thesis work. I would like to express my deepest gratitude to my beloved family, particularly my father Dereje M. Duresa and my mother Berhane Yadesa, for their unwavering support, love, and daily prayers. Their moral guidance and encouragement have been constant sources of strength and motivation throughout my academic journey. I am truly thankful for their belief in me and their desire for my happiness and success.

I extend my gratitude to Adama Science and Technology University, School of Applied Natural Science, Department of Applied Physics Program, for providing me with a grant that has financially supported me in carrying out this thesis work. Their support has been invaluable in facilitating the completion of this thesis. Lastly, I would like to express my deep appreciation to Mizan-Tepi University for granting me the opportunity to pursue my studies and enabling me to achieve my academic goals. In conclusion, I am profoundly thankful to all individuals who have played a part, directly or indirectly, in the completion of this thesis. Your unwavering support, guidance, and contributions have been pivotal in shaping this research work. It is with immense gratitude that I acknowledge your contributions and express my heartfelt appreciation.

CONTENTS

LIST OF TABLES

LIST OF FIGURE AND ILLUSTRATION

LIST OF ACCRONYMS AND ABBREVATION

AGN	Active Galactic Nuclei
BLR	Broad-Line Region
CFHTLS	Canada–France–Hawaii Telescope Legacy Survey
CIGALE	Code Investigating GALaxy Emission
DMH	Dark Matter Halos
eFEDS	The eROSITA Final Equatorial-Depth Survey
eROSITA	extended ROentgen Survey with an Imaging Telescope Array
NIR	Near-Infrared
NLR	Narrow-Line Region
QSO	Quasi-Stellar Object
RPS	Ram-pressure Stripping
SDSS	Sloan Digital Sky Survey
SED	Spectral Energy Distribution
SFR	Star Formation Rate
SMBH	Supermassive Black Hole
SRG	Spektrum-Roentgen Gamma
VIKING	VISTA Kilo-degree Infrared Galaxy
VIMOS	VIsible Multi-Object Spectrograph
VIPERS	VIMOS Public Extragalactic Redshift Survey
VISTA	Visible and Infrared Survey Telescope for Astronomy
WISE	The Wide-field Infrared Survey Explorer

ABSTRACT

In this study, we investigated the influence of host galaxy properties on X-ray active galactic nuclei (AGN) clusters using multiwavelength data. We utilized X-ray data from the eFEDS main catalog, optical and near-infrared data from the fourth data release of KiDS/VIKING, and mid-infrared data from WISE. By integrating these datasets and employing the CIGALE code, we estimated the star formation rate, luminosity, and stellar mass of the host galaxies. Our analysis reveals significant associations between luminosity, stellar mass, and star formation rate, providing valuable insights into AGN activity. Furthermore, we compare AGN clusters with non-AGN clusters to uncover distinctive characteristics. We found that AGN clusters exhibit differences in their population across various luminosity levels. Interestingly, a significant proportion of AGN clusters is concentrated in the middle range of luminosity $(45 < log L_{(0.5-2.0\ keV)} < 46)$ *for both low and high redshift classifications. In additions, we observed that galaxies hosting AGNs detected in X-ray emission tend to fall within a specific range of stellar mass (10-11 measured in* $log\ (M_{\star}(M_{\odot})$*. This stellar mass range is populated by a substantial number of AGN galaxies, irrespective of their redshift classification. Moreover, a significant population of X-ray AGN is concentrated within the star formation rate range of 1.5-2.5 (expressed in* $log\ (M_{\odot}yr^{-1})$*) in both low and high redshift regions. By analyzing the dependencies on luminosity, stellar mass, and star formation rate, this study provides valuable insights into the correlation and relationship between AGN clusters and their host galaxies. The comparison with non-AGN clusters and the integration of multiwavelength data from eFEDS, KiDS/VIKING, and WISE enhance the depth of analysis, contributing to a comprehensive evaluation of AGN clusters. These findings advance our understanding of the complex relationship between AGN clusters and host galaxy properties in the field of astrophysics.*

Keywords: *Active galactic nuclei (AGN), Host galaxy properties, Luminosity, Stellar mass, Star formation rate, non-AGN clusters.*

CHAPTER ONE

INTRODUCTION

1.1 Background of the Study

Inside the middle of almost every active galaxy, there is a supermassive black hole (SMBH). The accretion onto the SMBH releases huge quantities of energy across the complete electromagnetic spectrum from the so-called active galactic nucleus (Pouliasis et al., 2022). During the first half of the twentieth century, photographic observations of nearby galaxies detected a few function signatures of Active Galactic Nuclei (AGN) emission, despite the fact that there was not yet physical knowledge of the character of the AGN phenomenon. Some early observations protected the primary spectroscopic detection of emission traces from the nuclei of NGC 1068 by Edward Fath (Fath et al., 1909).

In 1909, Edward Fath conducted a study at Lick Observatory, examining the spectra of spiral nebulae and globular clusters to deepen our understanding of their continuous spectra. Vesto Slipher confirmed the presence of these lines in 1913 and revisited NGC 1068 in 1917 at Lowell Observatory, making spatially resolved observations and uncovering evidence of rotation (Slipher et al., 1917). Furthermore, Heber Curtis's invention of the jet in Messier 87 played a crucial role in describing 762 nebulae and clusters photographed with the Crossley Reflector (Curtis et al., 1918).

Although emission lines originating from the centers of galaxies were observed as early as the 20th century, it took more than half a century to fully comprehend the nature of these sources now known as AGN. Seyfert (1943) systematically studied galaxies with nuclear emission lines, leading to the coining of "Seyfert galaxies." However, it took many years before the true nature of these sources became established. The early 1950s witnessed significant developments in radio astronomy, renewing awareness of AGN (Edge et al., 1959).

AGN are the most prominent continuous X-ray sources in the extragalactic sky. The X-ray emission originates from a component of AGN called the Corona, located near the supermassive black hole, through inverse-Compton scattering of optical/UV photons from the accretion disk by electrons within the plasma (Kamraj, 2022).

X-ray observations provide an effective tool to investigate the physical conditions within the central engine of AGN (Beckmann et al., 2007).

The advent of X-ray astronomy in the 1960s and 1970s offered a more comprehensive understanding of the nature of AGN. The first successful X-ray observations of AGN were performed in the 1960s with rocket and balloon experiments, detecting emission from the bright quasar 3C273 (Bowyer et al., 1970). The Uhuru catalog, the first large assembly of X-ray sources(Giacconi et al., 1974), identified the three brightest AGNs in the X-ray sky.

Developing evidence from the past ten years suggests that galaxies and the supermassive black holes that exist within them are growing at the same time (Delvecchio et al., 2014; Dickinson et al., 2003; Koutoulidis et al., 2022). To differentiate between the potential contribution from the host galaxy and the prospective contribution from the AGN, Delvecchio et al. (2014) used a broad-band spectral energy distribution decomposition. From a far-IR perspective, they showed the connection between the AGN bolometric luminosity function and the supermassive black hole expansion rate throughout cosmic time up to $z\sim3$. The features of the host galaxy, such as the mass of the bulge, parameterized by luminosity or velocity dispersion, are also strongly correlated with the black hole mass (Merritt & Ferrarese, 2001; Yang et al., 2019).

Based on observational and theoretical models, several studies assume a connection between AGN and their host galaxies. Clustering analysis is one method to address the interconnections between black hole (BH) properties (e.g., BH mass, Eddington ratio) and host galaxy properties, such as star formation rate (SFR) and stellar mass ($M_\star$). Mountrichas et al. (2019) employed this method and found that host galaxy properties contribute to AGN clusters. However, obtaining statistically robust measurements regarding the dependence of AGN environments on these host galaxy properties requires X-ray samples several orders of magnitude larger than those used in previous studies. Therefore, we selected the latest X-ray survey data, eROSITA Final Equatorial-Depth survey (eFEDS), for our clustering analysis.

1.2 Statement of the Problem

X-rays are a highly reliable method for detecting AGN for several reasons. First, X-ray emission from AGN is observed to be nearly universal. Second, X-rays have the ability to penetrate through significant column densities of gas and dust, especially at higher X-ray energies. Lastly, the X-ray emission originating from processes within the host galaxy is typically weaker compared to that of the AGN itself. Based on these advantages, numerous studies have claimed a connection between AGNs and their host galaxies through X-ray observational evidence. One aspect of interest is the correlation between the mass of the supermassive black hole (SMBH) and the properties of its bulge, as parametrized by luminosity (Yang et al., 2019). Previous studies have focused on exploring the relationship between AGN clustering and X-ray luminosity to gain insights into the connection between AGN and host galaxy properties. For instance, Mountrichas et al. (2016) suggested a negative dependence of AGN clustering on luminosity, while other studies proposed a weak dependence, and some even suggested no statistically significant dependence and their results contradict each other (Coil et al., 2009).

Recent studies have provided valuable information on the luminosity dependence of X-ray clustering with respect to SMBH mass. However, until Mountrichas et al. (2019) pointed out the dependence of X-ray AGN clustering on parameters such as star formation rate (SFR), stellar mass ($M_{\star}$), and specific star formation rate (sSFR) by utilizing X-ray AGN data from the XMM–XXL area and cross-correlating it with galaxies in the VIPERS field, the clustering dependence of X-ray AGN on host galaxy properties had not been directly studied. One of the key challenges in studying the AGN clustering dependence on the host galaxy's properties, as highlighted by Mountrichas et al. (2019), is the lack of large-scale environment data for X-ray AGN across all their parameter space and uncovering its dependence on all host galaxy properties. Therefore, to overcome this problem and investigate the AGN clustering dependence on the host galaxy's properties, our work utilized the advanced X-ray survey data from the eROSITA Final Equatorial-Depth survey (eFEDS), which covers the large-scale environment of X-ray AGN.

1.3 Objective of the Study

1.3.1 General Objective

The general objective of this thesis is to investigate the contribution of host galaxy properties in X-ray AGN clusters.

1.3.2 Specific Objective

The specific objectives of this thesis are:

- To study the dependence of the x-ray AGN on luminosity.
- To study the dependence of the x-ray AGN on stellar mass.
- To study the dependence of the x-ray AGN on the star formation rate (SFR).
- To compare the AGN galaxy clusters with normal galaxy clusters.

1.4 Significance of the Study

The significance of this study is its ability to fill important gaps in knowledge and practice regarding the connection between AGN and their host galaxies using X-ray observations. By conducting this thesis, we clarify existing findings and gain fascinating insights into how X-ray clustering depends on different properties of the host galaxy. This is particularly important for our university, as we have recently started focusing on this field of specialization. This research will not only advance science but also showcase our institution's progress in this field. Furthermore, this study will serve as a strong research foundation, encouraging further exploration and discoveries in this domain, thus solidifying our commitment to pushing the boundaries of knowledge in this exciting area of astrophysics.

1.5 Outline of the Thesis

This thesis has been organized into five chapters. Chapter one sets the foundation by providing the background, stating the problem, outlining the objectives, and emphasizing the significance of the study. Chapter two conducts a comprehensive literature review, covering galaxy clusters, the role of the environment in galaxy evolution, the unified model of AGN, and prior studies on AGN in the x-ray band. This chapter establishes the existing knowledge in the field. Chapter three explores in detail the methodology, detailing the data sources, materials, and software utilized, as well as the data reduction and processing techniques employed. It also describes the specific analysis method, such as SED fitting with CIGALE, used to explore the relationship between host galaxy properties and x-ray AGN clusters. Chapter four presents the results and discussion, highlighting the findings obtained from the analysis. It thoroughly examines the contribution of host galaxy properties to x-ray AGN clusters, providing valuable insights into their interdependence. Finally, chapter five concludes the thesis by summarizing the key findings, emphasizing their implications, and offering recommendations for further research in the field. This organizational structure enables a comprehensive investigation of the connection between host galaxy properties and x-ray AGN clusters, leading to a deeper understanding of these phenomena.

CHAPTER TWO

LITERATURE REVIEW

2.1 Galaxy Clusters

Galaxy clusters are some of the biggest structures in the Universe that are held together by gravity. They consist of hundreds to thousands of galaxies and have masses ranging from about $10^{14} - 10^{15}$ times the mass of our Sun (Falco et al., 2014). These clusters form when the largest dense regions in the early Universe collapse under the force of gravity. This process is accompanied by incredibly energetic events, second only to the Big Bang itself. It also involves the interplay between the forces of gravity causing the collapse and the processes that lead to the formation of galaxies. Galaxy clusters are like crossroads where cosmology (the study of the Universe) and astrophysics meet. They provide valuable opportunities to test and understand theories about how structures in the Universe form, how galaxies evolve over time, the properties of the space between galaxies (intergalactic medium), and the behavior of plasma (a hot, ionized gas) in these extreme environments (Rosati et al., 2002).

Galaxy clusters can be distinguished from star clusters, such as open or globular clusters, based on their characteristics and location within the cosmic hierarchy. Star clusters are structures composed of stars that exist within galaxies. Open star clusters are typically found in the disk of galaxies, while globular clusters can be found in both the halo (outer region) and bulge (central region) of galaxies, orbiting around them. On the other hand, when a small number of galaxies, up to around 50, are found in close proximity, they are referred to as a group. When multiple galaxy groups come together and aggregate, they form larger structures known as galaxy clusters. Examples of galaxy clusters within the relatively local Universe include the Virgo cluster and the Coma cluster. These clusters serve as valuable examples for studying the properties and behaviors of galaxy clusters. Moreover, the clustering of galaxy clusters itself leads to the formation of even larger systems called superclusters. Superclusters are massive collections of galaxy clusters that exhibit a higher level of organization in the cosmic web (Amado, 2021).

Galaxy clusters consist of hundreds to thousands of galaxies, along with hot intergalactic gas emitting X-rays and substantial amounts of dark matter. They typically span a diameter of 2 to 10 megaparsecs (Mpc), which is a unit of distance used in astronomy, and the member galaxies within them exhibit a velocity dispersion ranging from about 100 to 1400 kilometers per second (km/s) (Lang, 2013). These characteristics contribute to the rich and complex nature of galaxy clusters and make them fascinating subjects of study in the field of astrophysics. Therefore, by connecting our thesis topic to the literature on galaxy clusters, we establish a foundation for investigating how host galaxy properties contribute to the formation and behavior of X-ray AGN clusters within these intriguing cosmic structures.

2.2 Environment as a Driver of Galaxy Evolution

The Universe is not uniformly distributed with galaxies but rather exhibits a structured pattern referred to as the cosmic web. This web consists of interconnected regions of matter, forming a network-like structure. Galaxy clusters, which are areas of high galaxy density, are found at the nodes of this cosmic web. These clusters gather galaxies together, creating concentrated regions within the vast expanse of the Universe. In addition to clusters, the cosmic web is also composed of filaments. These filaments serve as bridges, connecting galaxy clusters and forming a network throughout the Universe. Within these filaments, galaxies and smaller galaxy groups can be found (Kleiner et al., 2021).

These filaments act as pathways or conduits, allowing for the flow of matter and galaxies between clusters. Contrasting with the clusters and filaments are the cosmic voids. Despite their name, these voids still contain galaxies; however, the number density of galaxies within these regions is exceptionally low compared to the clusters and filaments. The voids represent vast, relatively empty spaces within the cosmic web. They are characterized by a scarcity of galaxies, contributing to the overall contrast and structure of the cosmic web(Pan et al., 2018).Different galactic environments provide different mechanisms acting upon a galaxy throughout its evolution. the morphology of a galaxy was dependent upon the galaxy density of the environment. In dense environments, such as the cores of clusters, galaxies are more likely to be early type, whereas in less dense environments late-type galaxies are more common. Furthermore, galaxies in denser environments tend to have older stellar populations than those in less dense environments (Thomas et al., 2005)

Within the dense, virialized cores of galaxy clusters, the intra-cluster medium (ICM) can reach extremely high temperatures, on the order of megakelvin. At such temperatures, the kinetic energy of the ICM makes it highly unlikely for gas to accrete onto the gravitational potential well of a galaxy. This means that the process of gas replenishment for a galaxy within the cluster is hindered. Furthermore, the presence of a massive galaxy's typical gas halo and satellite remnants can be lost in the cluster environment. This loss of gas clouds and satellite remnants prevents the replenishment of the galaxy with cold gas. As a result, once the galaxy has depleted its gas reserves, a process known as "strangulation" occurs, leading to a significant decline in star formation activity and an aging stellar population. Essentially, the galaxy's ability to form new stars is effectively halted (Davies et al., 2017).

The process of strangulation can be exacerbated by ram-pressure stripping (RPS), which occurs when the gas is stripped from a galaxy as it falls into the cluster. This stripping of gas happens before the galaxy reaches an environment where strangulation becomes the dominant mechanism. Consequently, the gas supply of a galaxy is already depleted by the time it enters an environment where strangulation is prevalent, further impeding its ability to sustain star formation (Masters et al., 2018).

Beyond the dense, virialized core of galaxy clusters, the population of galaxies consists of a mixture of infalling and backsplash galaxies. In this region, the galaxy density is such that interactions between galaxies at relatively low speeds are more common. These interactions can have significant effects on the gas distribution within a galaxy, consequently influencing its star formation and nuclear activity. Two key processes that can be triggered by these interactions are harassment and mergers. Harassment refers to the gravitational disturbances experienced by a galaxy as it interacts with other nearby galaxies. Such disturbances can disrupt the gas distribution within the galaxy, impacting its star formation and nuclear activity. Mergers, on the other hand, occur when two or more galaxies collide and merge together, potentially leading to dramatic changes in the gas content and structure of the galaxies involved (Pandey et al., 2022).

Ram-pressure stripping (RPS) also plays a role in this region outside the core of clusters. RPS refers to the process where the gas surrounding a galaxy is stripped away as it moves through the intra-cluster medium. This stripping can alter the morphology of galaxies, particularly spiral galaxies, as it causes the stellar disk component to thicken. Additionally, the stripping of gas can result in the formation of turbulent gas tails trailing behind the galaxy. As the galaxy falls toward the center of the cluster, where the ram pressures are most intense, star formation can occur within these turbulent gas tails. This phenomenon has been dubbed "Jellyfish galaxies" due to their resemblance to the marine organisms of the same name(Ebeling et al., 2014; Pitk, 2020).

Galaxy groups are smaller-scale structures that serve as the low-mass counterparts to galaxy clusters. Within these group environments, various interactions between galaxies can occur, influencing their star formation activity. In particular, compact groups of galaxies have been observed to trigger star formation through the interactions between their member galaxies. However, the group environment can also have the opposite effect by quenching or suppressing star formation in galaxies. This is achieved through processes such as ram-pressure stripping (RPS) and tidal interactions. RPS refers to the stripping of gas from galaxies as they move through the intra-group medium, depleting their gas reservoirs and inhibiting further star formation. Tidal interactions occur when the gravitational forces between galaxies in close proximity cause distortions in their shapes and disrupt their gas content, leading to a suppression of star formation(Scudder et al., 2012; Crossett et al., 2017).

Galaxy pairs, on the other hand, provide a unique setting to study the effects of interactions on galaxies that are either in the process of merging or will merge in the near future. These pairs offer a laboratory-like environment within a range of large-scale surroundings. Studies have shown that galaxies in pairs exhibit enhancements in star formation, likely due to the gravitational interactions between the pair members. Additionally, these galaxies are more likely to display morphological disturbances or irregularities in their structures as a result of the ongoing or imminent merger process (Ellison et al., 2010; Robotham et al., 2011).

We present in this literature, “environment as a Driver of Galaxy Evolution”, because the galaxy behavior and characteristics in group environments sheds light on the impact of interactions, mergers, and stripping processes on galaxy evolution. These processes significantly influence gas distribution, morphology, and star formation activity outside the core of galaxy clusters. Understanding these effects within diverse large-scale environments is essential for exploring the contribution of host galaxy properties to the formation and properties of X-ray AGN clusters. Furthermore, within galaxy clusters, high temperatures and the combined effects of strangulation and ram-pressure stripping lead to gas depletion and hinder active star formation. This understanding of the complex interplay between the intra-cluster medium and galaxy evolution is crucial for investigating the role of host galaxy properties in X-ray AGN clusters within cluster environments.

2.3 The Basic Unified Model of AGN

Antonucci (1993) proposed the first formalism for the fundamental unified model of AGN, which attributes the differences between observational classes of AGN to an orientation effect. According to this model, the varying perspectives from which the supermassive black hole (SMBH) and torus are observed along the observer's line of sight explain the observed differences. In the framework of the basic unified model, a typical AGN consists of several main components arranged in order from the smallest scales outward: the supermassive black hole, X-ray corona, accretion disk, broad line region, torus, and narrow line region. Figure 2.1 provides an overall schematic of an AGN, offering a perspective on the different components at various distances. Let's begin exploring the central engine in more detail.

The supermassive black hole (SMBH) is positioned at the core of an AGN and plays a pivotal role in generating the luminous emissions observed. Its energy originates from the gravitational in fall of surrounding matter. SMBHs are known to possess a mass range between $10^5 - 10^{10} M_{\odot}$. The linear size of the event horizon, which marks the boundary of the black hole, is directly linked to the mass of the SMBH. Typically, this size spans a range of approximately $10^{10} - 10^{15} cm$, equivalent to a few light-seconds to a few light-days in scale.

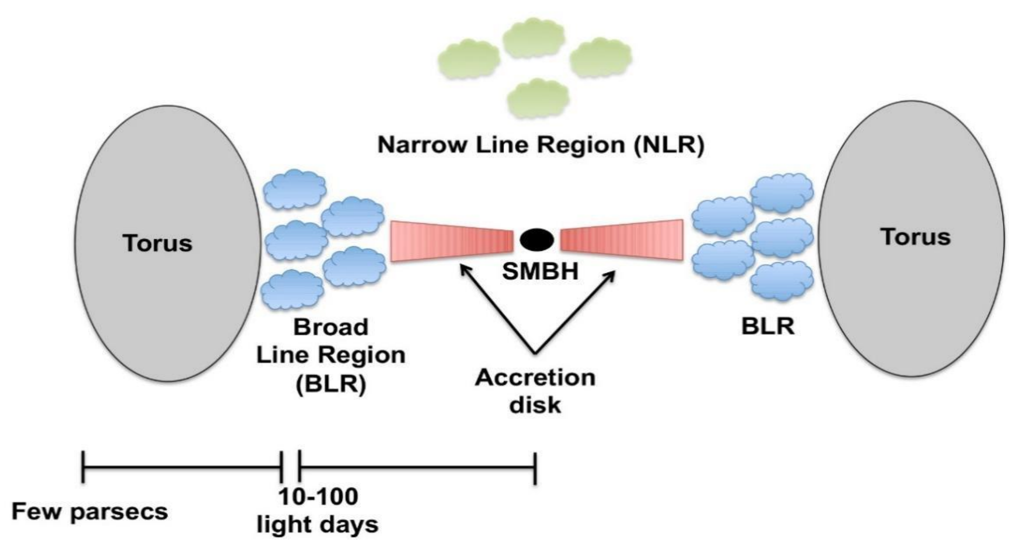

Figure 2.1: Schematic of AGN. Image credit: Claudio Ricci.

The accretion disk is a key component of an AGN and is often described as a geometrically thin, optically thick structure. It forms from the material that rotates in the vicinity of the SMBH. While the commonly used model assumes a thin disk, there are alternative models that propose slim or thick accretion disks, each providing insights into the nature of the disk. As matter spirals inwards towards the SMBH, it gradually loses angular momentum and is eventually accreted onto the black hole. This process leads to the conversion of gravitational energy into thermal radiation, manifesting as a blackbody spectrum. The accretion disk plays a crucial role in fueling the AGN's energy output and influencing its observed properties across various wavelengths.

The corona is another key component of an AGN, particularly located near the black hole. It consists of a hot plasma with low density and is believed to contain high-velocity electrons. The primary role of the corona is to up-scatter ultraviolet photons originating from the accretion disk to much higher energies, primarily in the X-ray band. This process, known as Compton scattering, results in the production of high-energy X-ray photons. The size of the corona is typically on the same scale as the event horizon of the black hole.

The broad-line region (BLR) is a region of gas surrounding the supermassive black hole that is strongly influenced by the central engine's energy output. The BLR consists of partially ionized, high-density clouds of gas that are free from dust. It takes on either a sphere-like or disk-like arrangement around the black hole. Due to the intense radiation from the central engine, the atoms in the BLR are photoionized, meaning they are ionized by absorbing energetic photons. The BLR emits broad emission lines, which are spectral features corresponding to permitted atomic transitions. These emission lines exhibit significant Doppler shifts, indicating that the gas is moving at velocities greater than 1000 km/s. The broadness and shifting of the emission lines provide valuable information about the dynamics and properties of the gas in the vicinity of the supermassive black hole.

The obscuring torus is a geometrically thick structure that extends perpendicular to the accretion disk, providing coverage of a significant portion of the sky as observed from the supermassive black hole (SMBH). While its exact shape remains uncertain, it is known to be inflated in the direction perpendicular to the accretion disk. The inner radius of the torus depends on the luminosity of the central source and can be as close as a few light months in the case of low luminosity AGNs.

On the other hand, determining the outer radius of the torus is more complex due to its clumpy nature, which makes it challenging to model accurately. Estimates for the outer radius range from a few parsecs to more extended two-component torus models that have a diffuse region extending hundreds of parsecs (Hönig, 2019).

The narrow-line region (NLR) is a bi-conical structure consisting of low-density ionized clouds that emit narrow permitted and forbidden emission lines. These emission lines are characterized by velocities below 1000 km/s. The NLR extends from the inner region of about a parsec from the AGN to hundreds of parsecs beyond it, making it the only component of an AGN that can potentially be spatially resolved. The kinematics within the NLR provide valuable insights into how the AGN luminosity and associated outflows may influence the host galaxy. For example, they can shed light on the impact of the AGN on star formation processes, including triggering or suppressing star formation activities (Revalski et al., 2021).

Relativistic jets are energetic outflows of particles that typically exhibit a bipolar and collimated structure, moving at relativistic velocities perpendicular to the accretion disk. These jets can be observed in certain AGNs and can extend over scales of millions of parsecs (Mpc) for particularly powerful jets. The emission from relativistic jets is predominantly non-thermal and is produced through processes such as synchrotron radiation and inverse-Compton scattering. Synchrotron radiation is responsible for the radio emission observed from all AGNs (Alexander et al., 2017). It occurs when relativistic electrons interact with a magnetic field, resulting in the emission of radio waves. The strength of this radio emission can vary between AGNs, with some being radio-quiet and others being radio-loud. Radio-loud AGNs are capable of generating collimated radio jets and lobes that extend throughout, and sometimes beyond, the host galaxy. These extended structures contribute significantly to the overall bolometric luminosity of the AGN system (Wilson & Colbert, 1995).

The presence of relativistic jets in AGNs plays a crucial role in shaping the properties and behavior of these active galaxies. Their energetic nature and ability to transport material and energy over vast distances have a profound impact on the surrounding environment. Understanding the formation, propagation, and impact of relativistic jets is essential for comprehending the full range of phenomena associated with AGN activity and their influence on the larger-scale structure of the universe.

This basic model provides an explanation for why narrow (permitted and forbidden) lines are observed in nearly all AGN, while broad lines are not: the former are emitted from larger spatial scales and are therefore observable from any orientation, while the latter originate from small scales and can therefore be hidden by the obscuring torus, depending on the observers' orientation with respect to the AGN. When the viewing angle is such that the innermost regions are seen directly, the observer sees a broad-line (type I) spectrum. If the same system is observed closer to edge-on orientation, where the obscuring torus hides emission from the accretion disk and the BLR, only a narrow-line (type II) spectrum will be observed. However, broad lines are, at least in principle, still observable in polarized light due to scattering on free electrons associated with the ionized NLR bi-cone (Antonucci, 1993).

2.4 Energy produced in AGN and Growth of SMBHs

2.4.1 Energy produced through Accretion

Energy is generated during the accretion of matter onto a central object, typically a supermassive black hole (SMBH) in the context of astrophysics. Accretion occurs when surrounding material, such as gas or dust, falls onto the gravitational well of the central object and forms an accretion disk. As the matter spirals inward towards the central object, it undergoes various physical processes, including friction and gravitational interactions, leading to the conversion of potential energy into kinetic energy and eventually into thermal energy and radiation. This conversion process releases a substantial amount of energy, contributing to the observed luminosity and activity of accreting objects, such as AGN and X-ray binaries (Pouliasis, Pouliasis, et al., 2020).

One key characteristic that distinguishes AGN from other sources within galaxies and beyond is their remarkable ability to emit an enormous amount of energy, reaching luminosities of up to 10^{46} $ergs\ s^{-1}$. Presently, it is widely accepted that AGNs contain a supermassive black hole at their core, which accretes matter from a surrounding disk. Within this framework, the energy released by AGNs is attributed to the conversion of gravitational energy into heat and radiation. Let us consider a scenario where a particle of mass dm, initially located at a considerable distance from the black hole (for simplicity, let's assume an infinite distance), becomes captured by the accretion disk and enters a circular orbit with a radius r around the black hole. In this situation, the mass particle dm experiences a centripetal force that maintains its equilibrium, and we can examine this balance more closely:

$$\frac{dmv^2}{r} = \frac{GMdm}{r^2} \quad 2.1$$

where M is the mass of the black hole. In the circular orbit, the particle has negative total energy. As the initial energy, E_∞, in its original position, was zero, the release of the extra energy, dE_{acc}, should be due to viscosity in the accretion disc:

$$dE_{acc} = E_\infty - E_r = 0 - \left(\frac{1}{2}dmv^2 - \frac{GMdm}{r}\right) \quad 2.2$$

From the equations 2.1 and 2.2 there is:

$$dE_{acc} = \frac{1}{2}\frac{GMdmv^2}{r} \quad 2.3$$

Considering the Schwarzschild radius of the black hole ($R_s = 2GM/c^2$), the previous equation gives:

$$dE_{acc} = \frac{1}{4}\frac{R_s dmc^2}{r} \quad 2.4$$

The luminosity, L_{acc}, produced by this accretion is:

$$L_{acc} = \frac{dE_{acc}}{dt} = \frac{1}{4}\frac{R_s}{r}\dot{m}c^2 \quad 2.5$$

where $\dot{m} = dm/dt$ is the accretion rate of the material into the black hole. The latter equation, further, can be written as:

$$L_{acc} = \eta\dot{m}c^2 \quad 2.6$$

where $\eta = (R_s/4r)$ denotes the efficiency factor that converts the potential energy to radiation. The efficiency factor may vary in the range between 6 and 42% (Krolik, 1999), as the accretion rate depends on the mass of the black hole and the distance (compactness of the source).

The highest possible value for the energy release in AGNs is achieved when the black hole is spinning at its maximum speed. AGNs commonly exhibit efficiency values, denoted by η, that are close to 10%. A well-known example is the AGN called 3C 273, which was studied by Marconi et al. in 2004 and Merloni in 2004. These observations align with studies of quasars, which have efficiency values ranging from approximately 6% to 30%, as reported by Davis and Laor in 2011 (Davis & Laor, 2011; Pouliasis, Pouliasis, et al., 2020).

To provide a point of comparison, the efficiency of hydrogen fusion converting into helium through thermonuclear reactions in a star's core is relatively low, with an efficiency denoted as $\eta = 0.007$. In contrast, the accretion process in AGNs proves to be an exceptionally efficient method for generating the immense amount of radiation observed at their centers. The vast radiation output cannot be solely attributed to nuclear reactions within stars. Notably, the efficiency factor is heavily influenced by the black hole's spin, and when the spin is significant, the energy released becomes significantly greater, as described by Shapiro and Teukolsky in 1983.

In the case of our own galaxy, the Milky Way, its relatively low luminosity compared to AGNs can potentially be explained by equation 2.6. This discrepancy arises from either a very low accretion rate or an exceptionally small efficiency process occurring within the Milky Way (Pouliasis, Pouliasis, et al., 2020).

2.4.2 Growth of SMBHs

Supermassive black holes (SMBHs) accumulate mass over time. SMBHs are extremely massive black holes found at the centers of galaxies, with masses ranging from millions to billions of times that of our Sun. The growth of SMBHs is a result of accretion, where surrounding gas, dust, and other matter are drawn towards the SMBH and form an accretion disk around it (Pouliasis, Pouliasis, et al., 2020). When considering a steady, spherically symmetric, and non-rotating accretion process of fully ionized gas, such as hydrogen, there exists a maximum achievable luminosity based solely on the mass of the accreting object, as described by Eddington in 1916. According to hydrostatic equilibrium, the Eddington luminosity, also known as the Eddington limit, is reached when the gravitational force equals the radiation pressure. The gravitational force acting on an electron-proton pair (interacting electromagnetically), with masses me and mp respectively, can be expressed as:

$$F_{grav} = \frac{GM(m_p + m_e)}{r^2} == \frac{GMm_p}{r^2} \qquad 2.7$$

Here, G represents the gravitational constant, M is the mass of the accreting object, and we assume the electron's mass to be negligible compared to the proton's mass ($mp = 2000me$). On the other hand, a photon with energy $h\nu$ and luminosity L has flux $L/4\pi r^2$, thus the number of the photons will be:

$$N_{phot} = \frac{L}{4\pi r^2 h\nu} \qquad 2.7$$

The radiation pressure related to the momentum transferred from photons to electrons is:

$$F_{rad} = \sigma_T N_{phot} p = \frac{\sigma_T L h\nu}{4\pi r^2 h\nu} \qquad 2.8$$

where $\sigma_T = 6.65 \times 10^{-25} cm^2$ is the Thomson scattering cross-section and the momentum is defines as $p = h\nu$. Satisfying the condition of the energy production, the radiation power should be lower than the gravitational force:

$$F_{rad} \leq F_{grav} \qquad 2.9$$

thus, by replacing these quantities with equations 2.7 and 2.9 the Eddington luminosity, L_{EDD}, can be given by:

$$\frac{\sigma_T L}{4c\pi r^2} \leq \frac{GMm_p}{r^2} ==> L_{EDD} \leq \frac{4\pi GMm_p c}{\sigma_T} = 1.26 \times 10^{38} \left(\frac{M}{M_o}\right) \text{erg/s} \qquad 2.10$$

So, the L_{EDD} is depending only from the mass of the accreting object. Theoretically, if the luminosity is higher than the L_{EDD}, then the ionized gas is expelled by the radiation pressure and the accretion will be halted resulting in a natural feedback process with a limiting accretion rate. This accretion rate, the Eddington accretion rate $\dot{M}_{EDD}$can be inferred by setting the accretion luminosity (eq. 2.6) equal to the Eddington luminosity (eq. 2.10):

$$\dot{M}_{EDD} = \frac{L_{EDD}}{\eta c^2} \sim 2.2 \left(\frac{M_{BH}}{10^8 M_o}\right) \left(\frac{\eta}{0.1}\right)^{-1} [M_o yr^{-1}] \qquad 2.11$$

Moreover, it is crucial for the Eddington ratio, defined as $\lambda_{Edd} = L_{Bol}/L_{Edd}$, to remain below unity, as accretion ceases for luminosities surpassing L_{Edd}. This ratio is believed to regulate the growth of supermassive black holes (SMBHs) throughout cosmic time, applying to both low and high redshifts. However, in reality, the accretion process exhibits a more axial rather than spherical symmetry, challenging the assumption made in this context. Consequently, there can be luminosities surpassing L_{Edd}, associated with super-Eddington accretion rates. Super-Eddington accretion periods are considered plausible, as suggested by Zubovas & King in 2013, and they may even be necessary to account for the rapid growth of the earliest SMBHs (Zubovas & King, 2013; Denis et al., 2017; Pouliasis, Mountrichas, et al., 2020).

2.5 The Role of AGN In Galaxy Evolution

2.5.1 Galaxy Growth

AGNs, in addition to being captivating phenomena, play a pivotal role in the evolutionary journey of galaxies. Through observations, a compelling correlation has been discovered between the mass of the central black hole and the velocity dispersion of the galactic bulge. This relationship finds support in the Faber-Jackson relation, which establishes a link between the velocity dispersion of early-type galaxies (which can be likened to the bulge component of late-type galaxies) and the luminosity of the bulge. The relation suggests that the mass of the bulge component is directly proportional to the mass of the black hole, assuming a certain mass-to-light ratio. This correlation reveals a coevolutionary association between supermassive black holes and their host galaxies. It implies that the properties of the black hole and the galaxy mutually influence each other during their respective evolution. The mass of the central black hole and the velocity dispersion of the galactic bulge are intertwined, reflecting the interconnected nature of these two entities. This discovery highlights the significance of studying the relationship between supermassive black holes and galaxies in order to gain a comprehensive understanding of their evolution (Gordon, 2018).

2.5.2 AGN Feedback

The accretion process onto the supermassive black hole (SMBH) in an AGN can have significant effects on the surrounding galaxy. Observations have revealed that AGN tend to occupy the "green valley" region of the color-mass diagram, indicating a correlation between AGN activity and suppressed star formation in galaxies. This phenomenon is believed to be responsible for shaping the high-mass end of the luminosity function. It is known as AGN feedback, which can occur through two modes: quasar-mode and radio-mode feedback, and sometimes both (Gordon, 2018).

Radio-mode feedback occurs when inefficient accretion processes generate jets that heat and remove gas, hindering star formation. In quasar-mode feedback, the gas required for star formation is heated through quasar winds, primarily in AGN that are efficiently accreting. However, it is important to note that the shocking and compression of gas caused by AGN activity can also lead to positive feedback by triggering star formation at larger distances from the AGN itself. These intricate feedback mechanisms play a crucial role in understanding the interplay between AGN and galaxy evolution (Ishibashi et al., 2014; Gordon, 2018).

2.5.3 Effect on the Galactic Environment

The influence of an AGN extends beyond its immediate host galaxy. The jets generated by the AGN, which are responsible for mechanical feedback within the galaxy, can extend to distances of a few megaparsecs and thus impact the surrounding galactic environment. This phenomenon is known as AGN feedback. One notable aspect of AGN feedback is its potential to address the cooling-flow problem in clusters. In clusters of galaxies, there is a discrepancy between the amount of gas expected to cool and condense in the cluster cores and the observed X-ray luminosities. AGN feedback plays a role in this by supplying energy to the intra-cluster medium, preventing the cooling and condensation of gas. This energy input from the AGN helps sustain the observed X-ray luminosities in the cores of galaxy clusters. By injecting energy into the intra-cluster medium, AGN feedback acts as a counterbalance to the cooling processes and helps regulate the overall gas dynamics in cluster environments. This mechanism has been extensively studied and is considered a significant factor in understanding the evolution and properties of clusters (Clarke et al., 2017).

2.6 Studies of AGN in the X-ray Band

X-ray observations provide a nearly complete selection of AGNs with low contamination from non-AGN systems. There are several reasons for this. Firstly, X-ray emission from AGNs appears to be nearly universal. Secondly, X-rays have the ability to penetrate through large column densities of gas and dust, especially at higher X-ray energies. Additionally, the X-ray emission from host-galaxy processes is typically weaker compared to that of the AGN itself. The intrinsic X-ray emission from AGNs is primarily attributed to processes associated with the accretion disk, while the jet also contributes significantly to the X-ray band. One of the main processes responsible for X-ray emission is the phenomenon known as inverse Compton scattering. In inverse Compton scattering, the high-energy electrons in the accretion-disk "corona" interact with lower-energy photons from the accretion disk. Through this interaction, the electrons gain energy from the photons, causing them to be scattered to higher X-ray energies (Brandt & Alexander, 2015).

However, the X-ray emission from AGNs is modified due to interactions with matter in the nuclear region. These interactions include processes such as reflection, scattering, and photo-electric absorption of photons from the accretion disk and/or the obscuring AGN torus. Depending on the geometry and inclination angle of the torus relative to the line of sight, the relative strength of these components can vary significantly from source to source, resulting in a wide range of X-ray spectral shapes(Alexander et al., 2017). Therefore, X-ray observations provide a valuable tool for studying AGNs as they offer a nearly complete selection of AGNs, with X-rays being able to penetrate through the surrounding gas and dust. The study of X-ray emission and its spectral characteristics helps in understanding the underlying processes and properties of AGNs.

2.7 Host Galaxy Properties of X-Ray AGN

Host galaxy properties of AGNs at various redshifts provide important clues for understanding the mechanisms that trigger AGN activities during different stages of the universe's evolution. For example, the mass of the dark matter halos (DMH) in which AGNs reside is linked to the lifetime of the black hole (BH) (Cappelluti et al., 2010). Furthermore, many authors have attempted to predict the clustering dependence of AGNs based on host galaxy properties, considering factors such as luminosity, stellar mass, and the star formation rate (SFR). We will review the effects of these properties on AGN clusters one by one.

2.7.1 The Luminosity of X-Ray AGN

Mountrichas et al. (2016), predicts evidence for a negative luminosity dependence of the AGN clustering. This is consistent with suggestions that AGN have a broad dark matter halo mass distribution with a high mass tail that becomes subdominant at high accretion luminosities. The northern tile of the wide-area and shallow XMM-XXL X-ray survey field is used to estimate the average dark matter halo mass of relatively luminous X-ray-selected active galactic nucleus $\left[logL_{X(2-10keV)} = 43.6^{+0.4}_{-0.4} erg\ s^{-1}\right]$ in the redshift interval $z = 0.5 - 1.2$ (Mountrichas et al., 2016).

Clustering studies of moderate-luminosity X-ray-selected AGN typically measure mean Dark matter halo(DMH) masses of $\approx 10^{13} h^{-1} M_{\odot}$,at least to $z \approx 1.5$ (Coil et al., 2009; Krumpe et al., 2015). When compared to UV/Optically selected powerful QSOs, it leads to a negative luminosity dependence of the AGN clustering, i.e., decreasing mean DMH mass with increasing accretion luminosity. Possible interpretations include different AGN triggering mechanisms or diverse accretion modes that dominate at different AGN luminosity regimes. There are also attempts to explore the luminosity dependence of the clustering using x-ray-selected AGN only. These, however, are met with moderate success(Fanidakis et al., 2013). Controversially, There are also claims for a positive correlation between x-ray luminosity and clustering but the statistical significance of those results is small (Koutoulidis et al., 2013).

A serious limitation is that current x-ray AGN samples are typically small in size. Statistical uncertainties, therefore dominate and do not allow clustering investigations over a sufficiently large luminosity baseline. This issue can be handled by joining clustering restrictions from x-ray samples with different depths and survey areas that probe different parts of the luminosity function at a given redshift. There are currently numerous x-ray surveys with sizes typically $\lesssim 2deg^2$ that give constraints on the statistical properties of moderate and low-luminosity AGN. In contrast, the number of wide-area x-ray samples that provide sufficient statistics at the bright end of the x-ray luminosity function is still limited (Mountrichas et al., 2016).

Mountrichas et al. (2016), estimate the average dark matter halo mass of a relatively luminous x-ray-selected active galactic nucleus. Preceded to the result, they use the galaxy spectroscopic sample from the VIPERS survey, which uses the VIsible Multi Object Spectrograph to perform deep optical spectroscopy over 24 deg^2 split between the W1 and W4 wide tiles of the Canada–France– Hawaii Telescope Legacy Survey (CFHTLS) and the X-ray-selected AGN sample is compiled from the XMM-XXL survey, which covers a total of about 50 deg^2 splits into two nearly equal area fields. The equatorial subregion of the XMM-XXL overlaps with the CFHTLS-W1 field and extends to about 25 deg^2. They limit the clustering analysis to X-ray sources in the redshift interval $0.5 < z < 1.2$. This is to allow cross-correlation with the VIPERS galaxy sample. X-ray luminosities are estimated in the 2–10 keV band assuming a power law X-ray spectrum with $\Gamma = 1.4$ for the k-corrections.

Finally, Mountrichas et al. (2016) provide evidence for a decreasing mean DMH mass for AGN with increasing accretion luminosity. These results are consistent with suggestions that the DMH mass distribution of AGN is broad and includes a massive-end tail, which skews measurements of the mean DMH mass of AGN to high values. This tail appears to become subdominant with increasing accretion luminosity They also discuss the results in the context of cosmological semi-analytic models in which the broad DMH mass distribution of AGN is related to different fueling modes of the central black hole and show that the observed negative accretion luminosity dependence of the X-ray AGN clustering is in qualitative agreement with such models (Mountrichas et al., 2016).

2.7.2 The Stellar Mass of X-Ray AGN

To study the dependence of the X-ray clustering on various properties of the host galaxy, i.e., $M_\star$, SFR, and sSFR. In each of these cases, the purpose is to study the dependence of AGN clustering on one parameter and at the same time avoid the degeneracy among the galaxy properties. To accomplish this, the various cuts applied are based on two criteria: (i) create nearly equal subsamples, and (ii) only one of the host galaxy properties differs between two subsamples, while the rest of the properties have similar median values. This allows us to attribute any clustering difference to the galaxy property under consideration. many studies attempt to show the correlation between AGN clustering and host galaxy properties (Mountrichas et al., 2019).

Mountrichas et al. (2019) used the PDR-2 of the VIPERS survey to cross-correlate X-ray AGN from the XMM–XXL field with the VIPERS galaxies and estimated the DMHM, this result agrees with the measurements of Mountrichas et al. (2016) that used the PDR-1 VIPERS data set. Accordingly, to study the dependence of clustering of X-ray AGN and normal galaxies on host galaxy properties, at $z \approx 0.8$.

They split 305 x-ray AGN samples into high- and low-M subsamples using two cuts, i.e., $\log\left({M_\star}/{M_\odot}\right) = 10.5, 10.8$. These cuts have been chosen because they create subsamples with very similar properties (SFR, redshift, and X-ray luminosity) and show a positive dependence between the AGN and galaxy clustering on $M_\star$ (Mountrichas et al., 2019).

Zou et al. (2019), show that the host galaxies of type 1 and type 2 AGNs have similar SFRs and cosmic environments in general, but the former tend to have a lower $M_\star$ than the latter. The difference in $M_\star$ indicates that the AGN unification model is not strictly correct, and both the host galaxy and torus may contribute to the optical obscuration of AGNs. Type 1 AGNs have slightly smaller $M_\star$ than type 2 AGNs even when z and L_X are controlled, and the difference is statistically significant ($\approx 4\sigma$). Test various sample-selection criteria and parameter settings in

Code Investigating GALaxy Emission (CIGALE) and find that type 1 sources always have slightly lower $M_\star$. Those trials support the reliability of the difference. This difference in $M_\star$ for type I versus type II AGNs indicates that spectral-type transformation is unlikely to be prevalent because frequent widespread transitions would average out any differences in host-galaxy properties (Zou et al., 2019).

2.7.3 The Star Formation Rate of X-Ray AGN

Based on observations in the nearby and early Universe, there is a conflict between different studies. In the low redshift regime, Shimizu et al. (2017) found that AGNs present enhanced star formation rate (SFR) compared to a control galaxy (non-AGN) sample. Based on their analysis, the SFR of AGNs shows a small dependence on AGN luminosity with no evidence for an upturn at high luminosities. Leslie et al. (2016) used SDSS sources at $z < 0.1$ and classified them based on their emission line ratios. They found that AGN feedback suppresses the star formation of the host galaxy. Caution has to be taken, though, when comparing results from different studies. AGNs constitute a diverse population, and different selection criteria choose AGN with different properties (Pouliasis et al., 2019; Pouliasis, Mountrichas, et al., 2020).

At higher redshifts, Florez et al. (2020) used x-ray-selected AGNs in Stripe 82 with $L_{(2-10keV)} > 10^{44}$ erg s^{-1} and compared their SFRs with non-X-ray galaxies at $0.5 < z < 3$. Based on their analysis, AGNs present 3-10 times enhanced SFR compared to non-x-ray systems.

Mountrichas & Shankar (2022) used X-ray AGNs in the Bootes, COSMOS and eFEDS fields, respectively, and compared their SFRs with that from reference galaxy control samples. They found that at $L_{2-10keV} < 10^{44}$ erg s^{-1} X-ray AGNs tend to have lower SFRs than that of star forming main sequence galaxies, while at higher luminosity AGNs present enhanced SFRs,at least for systems within a specific stellar mass, $M_\star$, range (Mountrichas et al., 2022).

At high redshifts ($z > 1$), galaxy (non-AGN) samples are limited in size. A number of studies have compared the SFR of X-ray AGNs with that of non-AGN systems. Towards this end, they estimated the sSFR. sSFR is defined as the ratio of the SFR of an AGN over the SFR of a star-forming MS galaxy with similar stellar mass and redshift as the AGN. These studies found that sSFR is independent of redshift (Mullaney et al. 2015), that the sSFR distribution of higher L_X AGNs is narrower and shifted to higher values compared to their lower L_X counterparts(Bernhard et al., 2019), that the effect of AGN on the SFR of the host galaxy depends on the location of the galaxy relative to the MS (Masoura et al., 2018) and that there is a strong correlation between the sSFR and the x-ray luminosity, with lower L_X AGNs to lie below the MS and higher L_X AGNs residing in host galaxies above the MS (Masoura et al., 2021)

2.8 AGN Selection Techniques

Alexander et al. (2017) conducted a comprehensive review of unique observational signatures related to clusters of galaxies. These clusters have been identified using various observational techniques, each providing valuable insights into their properties. Let's explore these techniques in more detail:

Optical or Infrared: Optical and infrared imaging and spectroscopy have proven to be effective in studying individual galaxies within clusters. To identify galaxy clusters, optical or infrared telescopes search for regions with higher densities of galaxies compared to their surroundings. Confirmation is achieved by identifying several galaxies at similar redshifts. Infrared searches are particularly useful for detecting more distant clusters at higher redshifts. The optical wavelength range typically refers to the visible light spectrum, which ranges from approximately 400 to 700 nanometers. On the other hand, the infrared spectrum extends beyond the red end of the visible spectrum and includes near infrared, mid infrared, and far infrared regions. Near infrared spans roughly from 700 to 2500 nanometers, mid infrared ranges from 2500 to 25,000 nanometers, and far infrared encompasses wavelengths from 25,000 to 1,000,000 nanometers. Different infrared wavelengths provide unique information about the composition, temperature, and properties of objects within the clusters.

X-ray: X-ray telescopes are utilized to detect the emission of x-rays from the hot plasma within clusters. By conducting x-ray imaging and spectroscopy, researchers can study the properties of the cluster gas. Cluster gas emits significant amounts of x-rays, making clusters prominent objects in x-ray surveys. In fact, clusters and AGN are among the brightest x-ray sources in extragalactic observations.

Radio: In addition to optical and x-ray observations, radio frequencies have also contributed to the study of galaxy clusters. Researchers have located diffuse structures emitting radio waves within clusters. Moreover, groups of radio sources, including both diffuse structures and AGN, have been employed as tracers to identify the locations of clusters. At higher redshifts, imaging around individual radio sources, such as AGN, has been employed to detect proto-clusters, which are clusters in the process of formation.

It's important to mention that the wavelength range of x-rays falls between approximately 0.01 and 10 nanometers. X-rays have shorter wavelengths and higher energy compared to optical and infrared radiation, allowing them to penetrate matter and provide insights into high-temperature phenomena. On the other hand, the radio wavelength range spans from millimeters to kilometers, making it significantly longer than optical, infrared, and x-ray wavelengths. Radio observations are valuable for studying low-energy processes, such as synchrotron radiation and molecular emissions, which can provide information about the properties of clusters and their constituent objects (Ragavan, 2021).

By addressing these points in my literature review, I emphasized the importance of employing multiple wavelength observations to obtain a more comprehensive view of clusters of galaxies. This multidimensional approach enabled us to uncover hidden details, reveal complex processes, and provide a deeper understanding of the universe's cosmic structures.

CHAPTER THREE

METHODOLOGY

3.1 Data Sources and Materials

3.1.1 The eROSITA Final Equatorial-Depth Survey (eFEDS)

The advantages of wide-field X-ray telescopes have been discussed for decades. However, most of the current generation of sensitive focusing X-ray telescopes, including the flagship observatories Chandra (NASA) and XMM-Newton (ESA), have a relatively small field of view, making it difficult to map large volumes of the Universe in a short amount of time. Therefore, eROSITA was designed as a sensitive wide-field X-ray telescope capable of delivering deep, sharp images over very large areas of the sky. Under that the eROSITA Final Equatorial-Depth Survey (eFEDS) is a project that aims to create a comprehensive X-ray survey of the entire sky visible from the northern hemisphere. This survey is being conducted using the eROSITA (extended ROentgen Survey with an Imaging Telescope Array) X-ray telescope, which was launched into space in July 2019 as part of the German-Russian Spectrum-Roentgen-Gamma (SRG) mission (Predehl et al., 2021; Brunner et al., 2022).

The eFEDs survey is designed to cover an area of the sky that is approximately 140 square degrees in size. The eROSITA telescope is capable of detecting X-rays with energies ranging from $0.2\,keV$ to $8\,keV$, and it can be producing detailed maps of the X-ray sky with unprecedented sensitivity and accuracy. The data collected during the eFEDS survey is being used to study a wide range of astrophysical phenomena, including the distribution of hot gas in clusters of galaxies, the properties of AGN, and the evolution of the large-scale structure of the universe. The survey is also expected to identify tens of thousands of new X-ray sources, many of which will be studied in detail by follow-up observations using other telescopes (Brunner et al., 2022).

The field coincides with an area enriched by deep optical and near infrared (NIR) imaging of the HSC2 Wide area Survey, KIDS-VIKING3, DESI Legacy Imaging Survey4, and, among others, GAMA5, WiggleZ, LAMOST6, and the SDSS7 spectroscopic coverage. A full description of the available multiwavelength data, together with the identification of the multiwavelength counterparts, is presented in (Salvato et al., 2022).

Based on these advantages, in our analysis, we use the X-ray sources observed in the eFEDS field; named as eFEDS main catalog which can provide information about source positions and extent, as well as fluxes. This catalogue includes 27,910 X-ray sources detected in the $0.2 - 2.3\ keV$ energy band with detection likelihoods ≥ 6, which corresponds to a flux limit of $\approx 7 \times 10^{-15}\ erg\ cm^{-2}\ s^{-1}$ in the $0.5 - 2.0\ keV$ energy range (Brunner et al., 2022).

3.1.2 The Kilo-Degree Survey (KiDS) and VISTA Kilo Degree Infrared Galaxy (VIKING) Imaging Survey

The galaxy population we used in our clustering analysis comes from the fourth data release catalogue of the $KiDS/VIKING$ imaging survey that has available optical and NIR photometry and photoz measurements for about 100 million galaxies over 1006 square degrees. The Kilo-Degree Survey (KiDS) is an ongoing optical wide-field imaging survey with the OmegaCAM camera at the VLT Survey Telescope, specifically designed for measuring weak gravitational lensing by galaxies and large-scale structure. When completed it will consist of 1350 square degrees imaged in four filters (ugri). For the first time, it includes photometry from the partner VIKING ESO public imaging survey on VISTA (Kuijken et al., 2019).

From the beginning, KiDS and VIKING were conceived together as a combined survey, covering the same parts of the sky. The VIKING survey started before KiDS, and was terminated in 2015 before completing the originally planned 1500 square degree footprint. It was therefore decided that KiDS observations would prioritise the 1350 square degrees for which VIKING data exist (Kuijken et al., 2019). For each of the 1006 square-degree survey tiles the data release includes calibrated stacked images in *u*, *g*, *r*, and *i* filters, their corresponding weights and masks, and single-band source lists extracted from the stacks. Furthermore, the multi-band ugriZYJHKs photometric catalogue covers 1006 square degree survey tiles, with PSF-homogenized and aperture-matched photometry and photometric redshift estimates(Kuijken et al., 2019).

3.1.3 The Wide-field Infrared Survey Explorer (WISE)

The NASA's Wide-field Infrared Survey Explorer launched in December 14th in 2009 aimed to map for the first time the entire infrared sky. WISE began surveying the sky on 2010 January 14 and completed its first full coverage of the sky on July 17.

The telescope with a weight of ~650 kg set in a polar circling orbit at ~525 km above the Earth. It carried a 40 cm diameter telescope with four infrared detector arrays on its focal plane. Each of the detectors has over a million pixels providing imaging photometry at 3.4, 4.6, 12 and 22 μm mid-infrared band passes (hereafter W1, W2, W3 and W4). WISE produce and release a reliable Source Catalog containing accurate photometry and astrometry for over 563 million objects (Wright et al., 2010)

3.1.4 Materials

In our work, we used CIGALE-v2022.1 to construct spectral energy distributions (SEDs) for our dataset. CIGALE (Code Investigating GALaxy Emission) is a Python-based software that models the emission from galaxies across the electromagnetic spectrum, from ultraviolet to radio wavelengths. To use CIGALE, we installed several necessary Python packages using Anaconda, including Astropy, NumPy, SciPy, Matplotlib, ConfigObj, and Rich. Astropy is a widely-used package for astronomical calculations, while NumPy and SciPy provide powerful numerical computing capabilities. Matplotlib is a popular package for data visualization, and ConfigObj is used to parse configuration files in CIGALE. Finally, Rich is a Python library for rich text and beautiful formatting in the terminal, which can be used for creating elegant command-line interfaces. Together, these packages enabled us to use CIGALE effectively in our work, and allowed us to analyze and visualize our results efficiently.

Additionally, Topcat software was used extensively for data analysis. Topcat is an interactive graphical viewer and editor for tabular data, which allows for the manipulation and visualization of large datasets. The software was utilized to exclude unnecessary objects from the datasets, match X-ray eFEDS with KiDS/VIKING and WISE data, convert AB magnitudes to flux, and generate figures to display the results. Topcat's powerful filtering and sorting capabilities made it possible to easily exclude unnecessary objects from the datasets, which is crucial in any data analysis process. Topcat's ability to match data from different sources and formats was essential in matching X-ray eFEDS with KiDS/VIKING and WISE data, and facilitated the integration of data from different wavelengths. The software's built-in flux conversion tools made it easy to convert AB magnitudes and flux in erg/cm^2 to flux in mJ, which allowed for the determination of the brightness of objects in the data and facilitated analysis. Finally, Topcat's visualization tools were used to create figures that presented the research results in a clear and concise manner.

Overall, the use of Topcat software in this thesis was an essential component of the data analysis process and played a critical role in the production of high-quality research results.

3.2 Data Manipulation and Processing

We have downloaded the eFEDS main catalog data from the web page at Max-Planck Institute for extraterrestrial Physics (MPE) dedicated to the eROSITA data release, which contains a large number of X-ray sources detected in a specific energy band. The catalog includes 27,910 sources that were detected with high detection likelihoods (≥ 6), which indicates a high confidence level in the detection. The corresponding flux limit for these detections is $\approx 7 \times 10^{-15}\ erg/cm^2$ in the $0.5 - 2.0\ keV$ energy range (Brunner et al., 2022). Next, we applied a filter called $EXT\_LIKE\ == 0$ to our dataset, which includes only point sources that were detected in the eFEDS field. This filter reduced the number of sources in our dataset to 27,369 or 98% of the main data. The reason why EXT_LIKE is necessary to apply is that it helps to remove extended sources, such as galaxy clusters or diffuse emission, from the dataset. These extended sources can contaminate the point source sample and affect the accuracy of the analysis. Therefore, by applying this filter, we can ensure that our dataset only includes point sources that are suitable for further analysis.

In a recent study by Salvato et al. (2022), multiwavelength counterparts and redshifts of X-ray sources were presented. To identify the optical counterparts of these sources, the DESI Legacy Imaging Survey DR8 (LS8) was used due to its homogeneous coverage of the field and its depth. The LS8 catalog also includes the Global Astrometric Interferometer for Astrophysics (Gaia) and WISE photometry. To find the counterparts of the X-ray sources, two independent methods were employed: NWAY and ASTROMATCH. NWAY is based on Bayesian statistics while ASTROMATCH uses the maximum likelihood ratio. Of the eFEDS point like sources, 88.4% were found to have the same counterpart identified by both methods. Each counterpart is assigned a quality flag, $CTP\_quality$, which is used to assess the reliability of the identification (Salvato et al., 2022).

Counterparts with $CTP\_quality\ \geq\ 2$ are considered to be reliable. This means that either both methods agree on the counterpart and have assigned a counterpart probability above the threshold ($CTP\_quality\ =\ 4$ for 20,873 sources), or both methods agree on the counterpart but one method has assigned a probability above the threshold ($CTP\_quality\ =\ 3$ for 1379 sources), or there is more than one possible counterpart (CTP_quality = 2 for 2522 sources). Totally in our work we used counterparts with $CTP\_quality \geq 2$ which is 24,774 in number. However, we note that sources with $CTP\_quality = 2$ represent only 5% (42 in number) of our final X-ray sample.

After the identification of the counterparts, to understand physical processes and populations, the different classes of objects need to be separated. The most important separation is between extragalactic sources (galaxies, AGN, Quasi-Stellar Objects (QSOs)) and galactic sources (stars, compact objects, etc.). In order to classify sources in the most reliable way, Salvato et al. (2022) have used a combination of methods and various information: spectroscopic, parallax measurements from Gaia, colours and morphology from imaging surveys. None of the methods is infallible because they all depend on the quality of the data (e.g., signal to nose ratio (SNR) for spectra, depth and resolution of images) and because of the degeneracy in colour-redshift space for many of the sources. They have therefore adopted a multi-step approach: at each step they extract from the pool of sources those that can be classified with high reliability either as extragalactic or Galactic. Of the 24,774 X-ray sources, 20,987 are characterized as extragalactic. Galactic sources are rejected from our analysis.

In order to classify extragalactic and galactic objects, a redshift flag is assigned to each source, CTP_REDSHIFT_GRADE. Only sources with CTP_REDSHIFT_GRADE ≥ 3 (20 987 of 24 774) are considered in this work. This criterion includes sources with either spectroscopic redshift (CTP_REDSHIFT_GRADE = 5) or for which the photoz estimates of the two methods agree (CTP_REDSHIFT_GRADE=4) or agree within a tolerance level (CTP_REDSHIFT_GRADE = 3; for more details, see Sect. 6.3 of Salvato et al. 2022).

About 3% of the sources are located at the borders of the field, which implies shorter exposure times, stronger vignetting, and higher background. These sources are excluded from our analysis ("inArea90" flag); this reduced our data into 20441. Additionally, we restrict our sources to those within the KiDS+VIKING area (Kuijken et al. 2019) to crossmatch with KiDS/VIKING data and also restricted our data in redshift range between $0.6 \leq z < 1.5$. Applying the redshift restriction and the KiDS/VIKING area criteria reduces the available number of X-ray sources to 4714 AGN for our analysis.

The KiDS/VIKING data utilized in this study was obtained from the ESO Science Archive. To ensure the consistency of the data, the redshift criteria were applied, limiting the range to $0.6 \geq z < 1.5$ to match that of the AGN sample and our KiDS/VIKING sample data becomes 27,443,972. To exclude sources that cover a different area than the AGN sample, TOPCAT software was utilized. After using TOPCAT software to exclude sources covering a different area than the AGN sample, our sample was reduced from 27,443,972 to 1,743,958 objects.

The eFEDS data or AGN sample was crossmatched with a galaxy sample. The purpose of this crossmatching was to explore the relationships between the AGN and the galaxies in the sample. The crossmatching process was carried out using TOPCAT software features, which allowed for efficient and accurate identification of matches between the different datasets.

After completing the initial crossmatching process, we continued their analysis by crossmatching the data with the WISE dataset. Then, our sample reduced to 1413 AGN sample. This additional crossmatching not only for extending our data up to mid infrared but also a more comprehensive understanding of the relationships between the AGN, galaxies, and their associated properties. The TOPCAT software was again used to carry out this crossmatching, and the resulting data was analyzed to identify any patterns or trends that could be relevant to the study.

Besides the AGN galaxy sample, to compare the Luminosity, stellar mass and SFR of X-ray AGN with non-AGN systems in a consistent manner, we compiled a galaxy (non-AGN) reference catalogue. We use the fourth data release catalogue of the KiDS/VIKING imaging survey (Kuijken et al. 2019), which has available optical and NIR photometry and photoz measurements for about 100 million galaxies over 1006 square degrees and the WISE All-Sky Data Release. We restrict the sample to those sources within the eFEDS region and apply the same requirements for photometric coverage of the X-ray sample. We also restrict the sample to sources with $0.6 \leq z < 1.5$. These requirements give us 240,676 galaxies.

3.3 Analysis
3.3.1 SED Fitting with CIGALE

We analyzed the multiwavelength data of our targets in order to measure the (host) galaxy properties of the sources; stellar masses, SFRs, and luminosities as well as to model the long-wavelength emissions from x-ray to mid-infrared. To this aim, we used the SED fitting code which is called Code Investigating GALaxy Emission (CIGALE) presented by (Boquien et al. 2019). CIGALE v2022.1 is built upon old version of CIGALE, and the fitting algorithm of CIGALE v2022.1 is the same as that of CIGALE. For a detailed description of the code, we refer to (Yang et al. 2022) and summarize below some of its main features.

CIGALE is a powerful multiwavelength spectral energy distribution (SED) fitting code for extragalactic studies and allows inclusion of the X-ray flux in the fitting process and has the ability to account for the extinction of the UV and optical emission in the poles of AGN (Boquien et al., 2019; Yang et al., 2022).

CIGALE is a program that enables users to enter a group of model parameters. The software then generates the model SED for every possible combination of the model parameters, and combines the model SED with filters to create model fluxes. By comparing the model fluxes to observed fluxes, the program calculates likelihood ($L = exp(-\chi^2/2)$) for each model. CIGALE has two types of analyses: maximum likelihood (minimum χ^2) and Bayesian. In maximum-likelihood analyses, CIGALE selects the model with the highest L value and computes physical properties such as Luminosity, stellar mass and star formation rate (SFR) based on this single model. In Bayesian-like analyses, CIGALE calculates the marginalized probability distribution function (PDF) for each physical property based on the L values of all models. Finally, CIGALE uses this PDF to derive the probability-weighted mean and standard deviation, which it outputs as the estimated value and uncertainty(Yang et al., 2022).

We used all the available photometry to construct the SEDs, from X-rays up to mid-infrared, and we created a grid that models both the galaxy and the AGN emission. In particular, sfhdelayed, bc03, nebular, dustatt_modified_CF00, dale2014, skirtor2016, x-ray, and red shifting models were utilized.

An increasingly popular way to model the SFH of galaxies is the so–called “delayed” SFH; according to this model the sudden onset of star formation and burst episodes in a double–

exponential parametrization may be too extreme in many practical cases where we expect the variation of the SFH to be smoother. Mathematically expressed:

$$SFR(t) \propto \frac{t}{\tau^2} \times \exp\left(-t/_{\tau}\right) for\ 0 \leq t \leq t_o \qquad 3.1$$

Where t_o the age of the onset of star formation, and τ the time at which the SFR peaks. Such a functional form has the advantage of providing a nearly linear increase of the SFR from the onset of star formation rather than other models (sfh2exp). After peaking at $t = \tau$, it smoothly decreases.

In addition to the SFH, we need to adopt a library of single stellar populations (SSPs). This technique is based on the property that stellar populations with any star formation history can be expanded in series of instantaneous starbursts, conventionally named 'simple stellar populations' (SSPs). The spectral energy distribution at time t of a stellar population characterized by a star formation rate $\psi(t)$ and a metal-enrichment law $\zeta\ (t)$ can be written as

$$F_{\lambda}(t) = \int_0^t \psi(t-t')\, S_{\lambda}[t', \zeta\ (t-t'\ )]\, dt' \qquad 3.2$$

We used the stellar population synthesis model of Bruzual & Charlot (2003) or bc03 which accurately predicts the spectral energy distribution (SED) of a galaxy based on its star formation history and metallicity, making it a widely used and well-tested model. The nebular model accounts for the effects of ionized gas on the SED of a galaxy, allowing for a more accurate estimation of physical properties. The dustatt_modified_CF00 and dale2014 models provide models for dust attenuation, with the latter being more flexible and physically motivated. Specially, the Dale et al. (2014) model utilized for implement the IR SED of the dust heated by stars (Yang et al., 2022).

In Figure 3.1, the dust emission is plotted in red, the AGN component in orange, the attenuated (unattenuated) stellar component is shown with the yellow (blue) solid (dashed) line, while the green lines show the nebular emission. The total flux is represented with black colour. Below each SED, we plot the relative residual fluxes versus the wavelength.

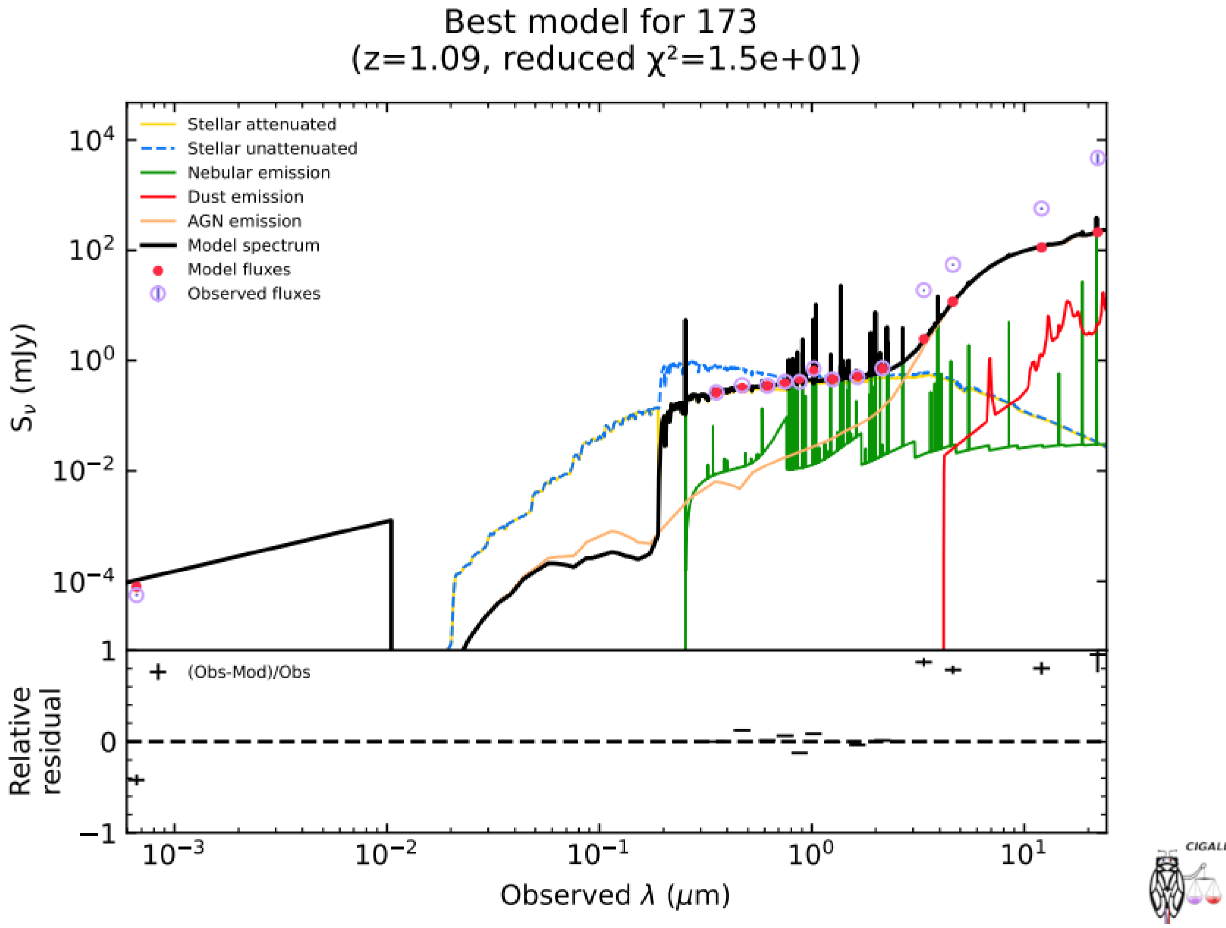

Figure 3.1: Examples of SED from sources used in our analysis.

Active galactic nucleus emission was modelled using the SKIRTOR templates. SKIRTOR is a clumpy two-phase torus model that considers an anisotropic, but constant, disk emission. The skirtor2016 model accounts for the effects of dust on the SED of a galaxy, providing more accurate estimations for galaxies with significant amounts of dust. The x-ray model provides a direct measure of the activity of the supermassive black hole in the center of a galaxy, which is crucial for understanding the evolution of galaxies. Finally, the red shifting model accounts for the effect of redshift on the observed SED of a galaxy, allowing for the estimation of physical properties at different redshifts. Overall, these models are essential for accurately estimating key parameters such as luminosity, stellar mass, and SFR, which are crucial for understanding the formation and evolution of galaxies (Stalevski et al., 2016). The full list of the models and their parameters used in our analysis are given in table 3.1. The constructed SED for our AGN sample is presented in Figure 3.1 for this study.

Table 3.1: Models and values for free parameters used by CIGALE in our work for the SED fitting.

Parameter	Value
Star formation history: delayed SFH with optional exponential burst	
e-folding time of the main stellar population model in Myr, τ_{main}	200, 500, 700, 1000, 2000, 3000, 4000, 5000
Age of the main stellar population in Myr	1500, 2000, 3000, 4000, 5000
Age of the late burst in Myr, age_{burst}	20
Mass fraction of the late burst population, f_{burst}	0.0, 0.005, 0.01, 0.015, 0.02, 0.05, 0.10, 0.15, 0.18, 0.20
e-folding time of the late starburst population model in Myr, τ_{burst}	50
Stellar population synthesis model	
Single Stellar Population Library	Bruzual & Charlot (2003) or bc03
Initial Mass function	1(Chabrier)
Metallicity	0.02
Nebular emission	
Ionization parameter ($log\ U$)	-2.0
Fraction of Lyman continuum escaping the galaxy (f_{esc})	0.0
Fraction of Lyman continuum absorbed by dust (f_{dust})	0.0
Line width (FWHM) in km/s	300
Dust attenuation: modified attenuation law Charlot & Fall (2000)	
V-band attenuation in the interstellar medium, Av_{ISM}	0.2, 0.3, 0.4, 0.5, 0.6, 0.7, 0.8, 0.9, 1, 1.5, 2, 2.5, 3, 3.5, 4
Dust template: Dale et al. (2014)	
AGN fraction	0.0
Alpha slope, α	2.0
AGN models from Stalevski et al. (2016) (SKIRTOR)	
Average edge-on optical depth at 9.7 micron (t)	3,7

Power-law exponent that sets radial gradient of dust density (pl)	1.0
Index that sets dust density gradient with polar angle (q)	1.0
Angle measured between the equatorial plane and edge of the torus (oa)	40
Ratio of outer to inner radius, $Rout/Rin$	20
Fraction of total dust mass inside clumps (Mcl)	0.97
Inclination angle (i)	30,70
AGN fraction	0.0, 0.1, 0.2, 0.3, 0.4, 0.5, 0.6, 0.7, 0.8, 0.9, 0.99
Extinction in polar direction, $E(B-V)$	0.0, 0.2, 0.4
Emissivity of the polar dust	1.6
Temperature of the polar dust (K)	100.0
The extinction law of polar dust	0(SMC)
X-ray module	
Photon index (Γ) of the AGN intrinsic X-ray spectrum	1.9
Maximum deviation of α_{ox}, $max\_dev\_\alpha_{ox}$	0.2
Deviation from the expected low-mass X-ray binary ($LMXB$).	0.0
Deviation from the expected high-mass X-ray binary ($HMXB$).	0.0

3.3.2 Quality and reliability examination of the fitting results

The technique gives a pair of estimates for each parameter that was determined through SED fitting. One estimate of a parameter corresponds to the likelihood-weighted mean value determined from its probability density function marginalized over all the other parameters (bayes value), while the other estimate of a parameter is generated using the best-fit model (best value). The weight is based on the likelihood, $exp\,(-\chi^2/2)$, associated with each model (Boquien et al., 2019). If there is a significant gap between both of the estimated value, the source should be excluded and the probability density function (PDF) is likely asymmetric or more complex shaped.

Therefore, to exclude sources with unreliable measurements from our analysis, we considered only sources with $1/5 \leq \frac{SFR_{best}}{SFR_{bayes}} \leq 5$ and $1/5 \leq \frac{M_{\star,best}}{M_{\star,bayes}} \leq 5$, where SFR_{best} and $M_{\star,best}$ are the best fit values of SFR and $M_{\star}$,respectively, and SFR_{bayes} and $M_{\star,bayes}$ are the Bayesian values, estimated by CIGALE.

This criterion reduces the number of X-ray sources to 1000. To further exclude systems with unreliable measurements of the (host) galaxy properties, we apply the same method presented in Mountrichas et al. (2021), which is based on visual inspection of the SEDs and we exclude badly fitted SEDs by taking in our work only sources which have the reduced, $\chi^2 < 5$. This criterion reduced our sample into 804(about 80% of the first data). Increasing the limit to $\chi^2 < 6$ adds more sources (around 7%) to our sample, but most of them have bad fits and thus unreliable host galaxy measurements. Reducing the threshold to $\chi^2 < 4$ would exclude additional sources, the vast majority of which have reliable fits. This criterion eliminates 82 AGN (8% of the sample).

3.3.3 Identification of non-X-ray AGN systems

As stated in Section 3.3.1, when we fit the galaxy reference catalogue using the SED fitting analysis, we also incorporate an AGN template (SKIRTOR). This allows us to measure the AGN fraction parameter, fracAGN, and identify systems with a significant AGN component. fracAGN is the ratio of the AGN's infrared emission to the galaxy's overall infrared emission $(1 - 1000\mu\, m)$. Galaxies with fracAGN > 0.2 are not included in the reference catalog. Approximately 99% of sources in the galaxy catalogue are rejected. This criterion has the potential to significantly impact our dataset by removing a substantial number of galaxies. As a result, it would considerably reduce the overall sample size. However, we can examine the implications of this criterion from two perspectives. Firstly, employing an alternative method may introduce errors that could potentially affect the identification of AGN. Secondly, this criterion demonstrates that our galaxy sample encompasses a substantial presence of AGN. In the broader context, our primary objective is to compare AGN and non-AGN populations, where the reduction in the number of non-AGN galaxies is not expected to have a substantial significant impact. In our work only 2889(about 1%) sources were included.

CHAPTER FOUR

RESULT AND DISCUSSION

In this chapter, we present the results of our study on the contribution of host galaxy properties on X-ray AGN clusters. The specific objectives of our study were to examine the dependance of AGN clusters on luminosity, stellar mass, and star formation rate, as well as to compare the AGN clusters with normal galaxy clusters. To achieve these objectives, we incorporated multiwavelength galaxy data from X-ray to mid-infrared to gain a comprehensive understanding of the properties of AGN clusters and employed the CIGALE code to estimate the star formation rate, luminosity, and stellar mass of the host galaxies. Generally, under this section we present the results of our analysis of the dependance of AGN clusters on luminosity, stellar mass, and star formation rate. We also compare the properties of AGN clusters with non-AGN clusters to gain insight into the unique features of AGN host galaxies.

To further investigate the dependence of AGN clusters on host galaxy properties, we divided our sample into two redshift subsamples, low redshift which consists 393 AGN population and high redshift which consists 411 AGN galaxies; these are ranging from 0.6 to 1.05 and from 1.05 to 1.5 respectively. This allowed us to control for the effects of redshift on our results and investigate whether the dependence of AGN clusters on host galaxy properties changes with redshift. We then cut the host galaxy properties, including luminosity, star formation rate, and stellar mass, into smaller pieces to investigate their effects on the AGN clusters.

4.1 Dependance of AGN Clusters on Luminosity

The dependance of AGN clusters on luminosity presented, to explore the relationship between AGN clusters and luminosity in order to understand their properties and behavior. To effectively analyze the dependence of AGN clusters on luminosity, we have divided the luminosity range into smaller, manageable bins for low and high redshift. This approach allows us to examine the characteristics and trends of AGN clusters across different luminosity levels with greater precision. By segmenting the data in this way, we can explore how AGN distributions or properties vary as luminosity changes.

Table 4.1: The properties of the X-ray AGN subsamples, using different Luminosity cuts.

	Low-redshift (0.6-1.05)			High-redshift (1.05-1.5)		
Luminosity ((log (ergs/s))	44-45	45-46	46-47	44-45	45-46	46-47
Mean of Luminosity (ergs/s)	44.782	45.508	46.198	44.913	45.749	46.22
Number of AGN	54	295	44	3	230	178
Mean of stellar mass (log (sol mass))	9.716	10.55	11.226	9.83	10.786	11.135
Mean of logSFR	1.864			2.362		
Total number of AGN	393			411		

Table 4.1 present our findings effectively and allows us to evaluated several key parameters in the various combination of redshift categories, within each luminosity bin. First, we have examined the population of AGN clusters, determining the number of clusters falling within each luminosity range and calculating the mean stellar mass in each luminosity bins. This provides insights into the distribution and abundance of AGN clusters and shows the stellar mass at different luminosity levels. Secondly, present the mean value of star formation rate to compare their values corresponds to high and low redshift.

As shown in table 4.1, Our analysis of AGN clusters at various luminosity levels has revealed significant differences in the population of AGN based on luminosity. Notably, we have observed that a large number of AGN clusters are concentrated in the middle range of luminosity $(45 < logL_{(0.5-2.0\ keV)} < 46)$ for both low and high redshift classifications. To understand these differences, we can examine the data in terms of percentages. At low redshift, in the $(44 < logL_{(0.5-2.0\ keV)} < 45)$ luminosity bin, there are 54 AGN out of a total of 393, accounting for approximately 13.7% of the population. In the $(45 < logL_{(0.5-2.0\ keV)} < 46)$ luminosity bin, there are 295 AGN out of 393, representing about 75.1% of the population.

Finally, in the $(46 < logL_{(0.5-2.0\ keV)} < 47)$ luminosity bin, there are 44 AGN out of 393, constituting around 11.2% of the population. Similarly, at high redshift, the $(44 < logL_{(0.5-2.0\ keV)} < 45)$ bin consists of 3 AGN out of 411, making up roughly 0.7% of the population. The $(45 < logL_{(0.5-2.0\ keV)} < 46)$ bin contains 230 AGN out of 411, accounting for approximately 55.9% of the population. Lastly, in the $46 < logL_{(0.5-2.0\ keV)} < 47)$ bin, there are 178 AGN out of 411, representing about 43.3% of the population. These percentages shed light on the distribution of AGN populations and highlight the variations observed across different luminosity bins.

When comparing the luminosity bins in the low and high redshift ranges, several important points emerge. Firstly, at low redshift, the majority of AGN clusters are concentrated in the $(45 < logL_{(0.5-2.0\ keV)} < 46)$ luminosity bin, accounting for 75.1% of the population. In contrast, at high redshift, the $(45 < logL_{(0.5-2.0\ keV)} < 46)$ luminosity bin remains the most populated, but to a lesser extent, with 55.9% of the population. Secondly, in both redshift ranges, the $(44 < logL_{(0.5-2.0\ keV)} < 45)$ luminosity bin exhibits the lowest population percentage. However, the difference between low and high redshifts is significant, with 13.7% at low redshift and only 0.7% at high redshift.

Lastly, the $(46 < logL_{(0.5-2.0\ keV)} < 47)$ luminosity bin shows significantly different population percentages at both low and high redshifts, with 11.2% and 43.3%, respectively. These comparisons suggest a shift in the distribution of AGN populations as redshift increases, with a decrease in the low luminosity range and an increase in the high luminosity range.

The results presented in this study provide valuable insights into the physical interpretation of AGN populations at different luminosity levels and redshifts. The high concentration of AGN clusters in the middle range of luminosity $(45 < logL_{(0.5-2.0\ keV)} < 46)$ suggests that this particular luminosity regime may play a crucial role in the formation and evolution of AGN. The observed differences in AGN populations at different luminosity levels could be attributed to various factors, such as the availability of gas reservoirs for accretion, the presence of AGN triggering mechanisms, and the interplay between AGN feedback and host galaxy properties. Additionally, the variations observed between low and high redshifts indicate that the evolution of AGN populations is influenced by the cosmic environment and the underlying physical processes occurring over cosmic time. Further investigations, including multi-wavelength studies and theoretical modeling, will be essential to deepen our understanding of these complex phenomena and their implications for galaxy evolution and the growth of supermassive black holes.

In the figure 4.1, we show the relationship between luminosity (L) and the number of AGN clusters correspond to redshift. where LR refers the lower redshift and HR refers high redshift; L1, L2, L3, L4 are the luminosity bins of our sample in range between ($44 < logL_{(0.5-2.0\ keV)} ergs/s < 47$). for example, LR_L1(green) shows the distribution of x-ray AGN galaxies in the low redshift those have less $< 45(\ in\ logL_{(0.5-2.0\ keV)} ergs/s)$ than luminosity.

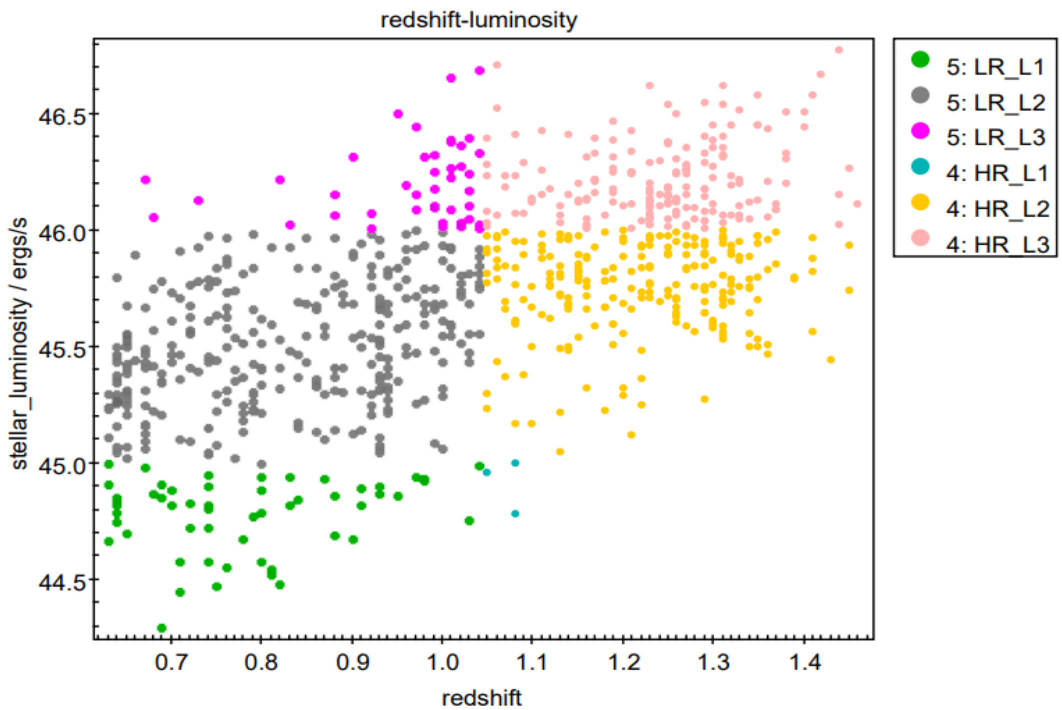

Figure 4.1: The distribution of x-ray AGN in redshift-luminosity plane.

In our analysis of AGN clusters at different luminosity levels, we have found a consistent increase in the mean value of stellar mass corresponding to increasing luminosity in both low and high redshifts. This positive correlation suggests that AGN with higher luminosities tend to be hosted by galaxies with larger stellar masses. However, a fascinating observation arises when comparing the mean stellar mass values of the lowest and highest luminosity bins to that of the middle bin. Surprisingly, the mean stellar mass in both the first and last ranges of luminosity approaches the value found in the middle range.

One possible implication for this convergence is the interplay between AGN activity and host galaxy properties. While it is generally expected that higher luminosity AGN would be associated with more massive host galaxies due to increased gas reservoirs and potentially enhanced accretion rates, there may exist a subset of AGN in the lowest luminosity bin that are hosted by galaxies with comparable stellar masses.

These AGN might exhibit unique characteristics or undergo distinct accretion mechanisms that allow them to maintain similar stellar masses despite lower luminosities. This Fascinating result suggests that there may be underlying factors influencing the relationship between AGN luminosity and stellar mass, beyond a simple linear correlation.

In conclusion, our analysis demonstrates a consistent increase in the mean value of stellar mass with increasing luminosity in AGN clusters at both low and high redshifts. However, the convergence of mean stellar mass values between the lowest and highest luminosity bins suggests the presence of additional factors influencing the relationship between AGN luminosity and stellar mass. Further investigations that account for redshift dependencies and involve larger and more diverse AGN samples will shed light on the intricate connections between AGN properties, host galaxy characteristics, and the broader context of cosmic evolution.

4.2 Dependance of AGN Cluster on Stellar Mass

The dependance of AGN cluster on stellar mass is very crucial thing in studying AGN in many perspectives' way. Therefore, in our work, to show their relationship and dependance we fellow the previous method which is employed for AGN cluster dependence on luminosity. The methods employed in this section, involving the division of our sample into low and high redshift subsets, followed by the segmentation of estimated stellar mass into small bins, has allowed us to effectively investigate the dependence of AGN clustering on stellar mass while reducing the potential impact of redshift on our analysis. By splitting the sample based on redshift, we can examine AGN populations across different cosmic eras, providing insights into the evolution of AGN clustering over time.

Furthermore, the subdivision of estimated stellar mass into small bins has enabled a detailed examination of the effect of stellar mass on the distribution of AGNs within each bin. This approach ensures that the influence of stellar mass on AGN clustering is not obscured by the averaging effect of larger mass intervals. Additionally, by calculating the mean star formation rate (SFR) at each stellar mass bin, we can investigate any correlations or trends between AGN activity and the SFR of the host galaxies. This way we can enhance the robustness and reliability of our findings, providing a comprehensive understanding of the dependence of AGN clusters on stellar mass.

Table 4.2 present our findings effectively and allows us to evaluated several key parameters in the various combination of redshift categories, within each stellar mass bin. First, we have examined the population of AGN clusters, determining the number of clusters falling within each stellar mass range and calculating the mean value of SFR at each bin. This provides insights into the distribution and abundance of AGN clusters at different stellar mass levels. Secondly, present the mean value of Luminosity to compare their values corresponds to high and low redshift.

Table 4.2: The properties of the X-ray AGN subsamples, using different stellar mass.

	Low-redshift (0.6-1.05)			High-redshift (1.05-1.5)		
Stellar mass (log $(M_\star(M_\odot))$)	<10	10-11	11-12	<10	10-11	11-12
Mean of Stellar mass (log $(M_\star(M_\odot)$)	9.746	10.549	11.23	9.847	10.737	11.024
Number of AGN	89	219	85	5	227	179
Mean of SFR	1.53	1.99	2.04	1.5	2.313	2.623
Mean of Luminosity(ergs/s)	45.69			46.05		
Total number of AGN	393			411		

Based on the results of our study, it was found that galaxies hosting AGNs) detected in X-ray emission tend to reside or be more prevalent within a specific stellar mass range. Specifically, the range of stellar mass considered in our study was between 10 and 11 (measured in $\log\,(M_\star(M_\odot)$. This range was found to be populated by a significant proportion of AGN galaxies, regardless of their redshift classification.

In the low redshift region, we found that the smaller stellar mass bins (9-10 in $\log\,(M_\star(M_\odot))$), constituting approximately 22.6% of the AGN population, exhibit a relatively lower representation. The middle stellar mass bin (10-11 in $\log\,(M_\star(M_\odot))$ stands out with the largest share, accounting for 55.7% of the AGN population. Surprisingly, the high stellar mass bins ($11 - 12$ in $\log\,(M_\star(M_\odot))$ have a relatively lower presence, comprising only 21.6% of the

AGN population. Moving to the high redshift region, we noticed a contrasting distribution. The smaller luminosity bins demonstrate a significantly reduced representation, constituting merely 1.2% of the AGN population. Similar to the low redshift region, the middle luminosity bin (10-11) dominates the AGN population, encompassing 55.2% of the total. However, in this case, the high luminosity bins (11-12) show a relatively higher presence, accounting for 43.5% of the AGN population.

The range of stellar mass considered in our study was between 10 and 11 (measured in log $(M_{\star}(M_{\odot})$ is found to be populated by a significant proportion of AGN galaxies, regardless of their redshift classification. In the low redshift subset (redshifts less than 1.05), approximately 55.7% of the AGN galaxies were found to be distributed within the specified stellar mass range. Similarly, in the high redshift subset, about 55.2% of the AGN galaxies were also populated within this range. This suggests that the distribution of AGN galaxies, in terms of their stellar mass, is consistently prominent within this specific range across both low and high redshift populations.

The physical interpretation of this finding could be that there is a preferred stellar mass range within which AGN activity is more likely to occur. Galaxies within this range might possess certain characteristics or conditions that promote the growth and activity of supermassive black holes at their centers, leading to the observed AGN emission in X-rays. The stability of this trend across different redshifts further indicates that the preference for a specific stellar mass range is not strongly influenced by cosmic time, at least within the redshift range studied.

In the figure 4.2, we show the relationship between stellar mass and the number of AGN clusters correspond to redshift. where LR refers the lower redshift and HR refers high redshift; M1, M2, M3, M4 are the stellar mass at different bins of our sample from 9-12$\left(measured\ in\ \log\left(M_{\star}(M_{\odot})\right)\right)$. for example, HR_M1(red) shows the distribution of x-ray AGN galaxies in the high redshift those have less 10(log$\left(M_{\star}(M_{\odot})\right)$) stellar mass.

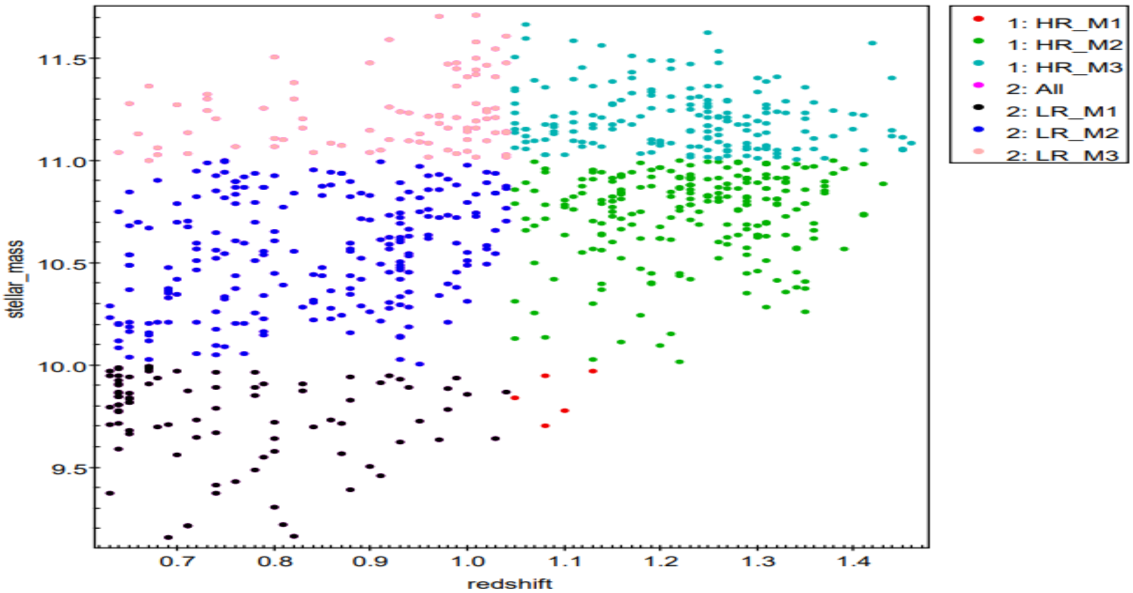

Figure 4.2: The distribution of x-ray AGN in redshift-stellar mass plane.

When comparing the first range (9-10 in log $(M_\star(M_\odot))$ of high redshift and low redshift, it was observed that the lowest stellar mass range was rarely populated by X-ray AGN galaxies, particularly in the high redshift subset. In contrast, a larger proportion of AGN galaxies were found within this lowest stellar mass range in the low redshift subset.

This finding indicates that, at the lower end of the stellar mass spectrum, the prevalence of X-ray AGN activity is more pronounced in galaxies at low redshifts while it is relatively rare in the high redshift population. Conversely, at higher end of the stellar spectrum, AGN galaxies more populated in the higher redshift while less populated in low redshift. The discrepancy in AGN population between the low and high redshifts within this lower stellar mass range and higher end range could be attributed to various factors associated with the evolution of galaxies and their black holes over cosmic time. It is possible that environmental effects, gas availability, or other triggering mechanisms differ between the two redshift regimes, resulting in a higher abundance of X-ray AGN galaxies within this particular stellar mass range in the low redshift subset and a scarcity in the high redshift subset. The another point we have seen from our result is the mean value of stellar mass at each bin is nearly approaches to the middle range values. for example, the mean value of galaxies stellar mass 9.746 and 11.3 for left and right range in low redshift classification respectively.

The analysis of the mean value of the star formation rate (SFR) at each bin provides insights into the relationship between SFR and stellar mass, considering different redshift regions. The results indicate a positive correlation between SFR and stellar mass in both redshift regions, suggesting that galaxies with higher stellar masses tend to exhibit higher levels of star formation.

However, when examining the impact of redshift on this relationship, some interesting patterns emerge. In the ranges of stellar mass 10-11 and 11-12, the mean value of SFR is found to be greater in the high redshift region compared to the low redshift region. This suggests that, for galaxies with stellar masses within these ranges, the star formation rates are generally higher at higher redshifts. It implies that the conditions or processes driving star formation are more conducive or active in galaxies at earlier cosmic eras.

Conversely, in the 9-10 range of stellar mass, the mean value of SFR is observed to be slightly lower in the high redshift region compared to the low redshift region. This suggests that, for galaxies within this specific stellar mass range, the star formation rates are somewhat lower at higher redshifts. It could imply that the factors influencing star formation in galaxies of this mass range differ between low and high redshifts, leading to variations in the observed mean SFR.

These findings highlight the complex interplay between stellar mass, redshift, and star formation rates in galaxies hosting AGNs. The positive correlation between SFR and stellar mass suggests that the availability of gas and the ability to form stars are influenced by the galaxy's mass. However, the impact of redshift indicates that additional factors related to cosmic evolution, such as gas supply, environmental conditions, or merger rates, play a role in shaping the observed SFR at different redshifts and stellar mass ranges.

4.3 Dependance of AGN Cluster on Star formation Rate

In this section, we examine the relationship between X-ray AGN clusters and the star formation rate (SFR). We employ the same methodology as in the previous section to investigate the impact of SFR on X-ray AGN clusters. Firstly, we categorize our AGN galaxies based on their redshift, dividing them into two groups: low redshift (less than 1.05) and high redshift (greater than 1.05). Next, we proceed to divide the SFR values into smaller intervals or bins. Subsequently, we determine the number of X-ray AGN falling within each bin and calculate the average SFR and luminosity values for these AGN.

This analysis allows us to assess the correlation between luminosity and SFR. Finally, prior to discussing our findings, we present the obtained results in Table 4.3, providing an overview of the estimated outcomes.

	Low-redshift (0.6-1.05)				High-redshift (1.05-1.5)			
SFR	-0.5-0.5	0.5-1.5	1.5-2.5	2.5-3.5	-0.5-0.5	0.5-1.5	1.5-2.5	2.5-3.5
Mean of SFR	0.08	1.23	1.96	2.665	-	1.381	2.199	2.696
Number of AGN	4	67	294	28	0	4	266	141
Mean of Luminosity(log(ergs/s))	44.777	44.88	45.557	46.282	-	44.947	45.794	46.265
Stellar-mass (log $M_{\star}(M_{\odot})$	10.515				10.93			
Total number of AGN	393				411			

Table 4.3: The properties of the X-ray AGN subsamples, using different SFR.

Our findings reveal several crucial points regarding the distribution of X-ray AGN with respect to the star formation rate (SFR). Notably, we observe that a significant population of X-ray AGN is concentrated within the SFR range of 1.5-2.5(expressed in units of log (($M_{\odot}$ /yr)) in both the low and high redshift regions.

This concentration suggests a favorable condition for the emergence of X-ray AGN within this particular SFR range.it implies that a particular range of star formation activity may contribute significantly to the triggering or fueling of AGN activity.

In the low redshift region, we observe an interesting trend where the population of X-ray AGN in the fourth SFR range (2.5-3.5) is nearly half that of the second range (0.5-1.5). Moreover, the first SFR bin (-0.5-0.5) exhibits a significantly lower number, with only four X-ray AGN. Interestingly, in the high redshift region, we find no AGN galaxies within the first SFR bin.

The concentration of AGN galaxies in the third and fourth bins (1.5-2.5 and 2.5-3.5, respectively) at high redshift warrants further investigation into the factors influencing AGN formation and evolution in these specific SFR ranges.

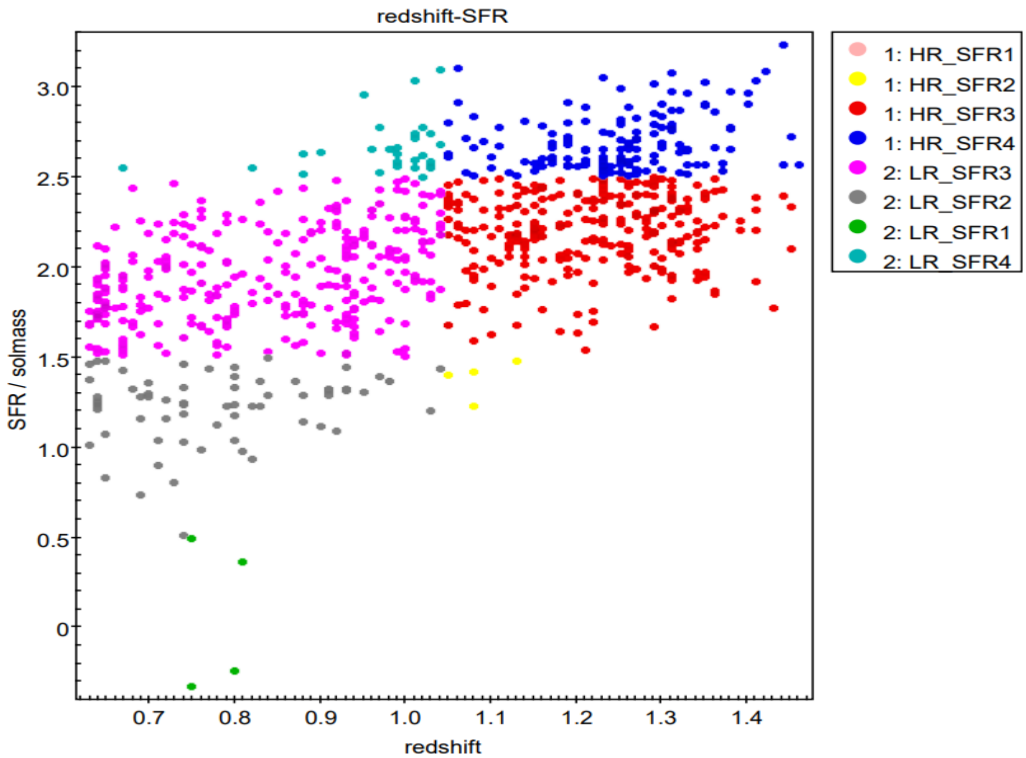

Figure 4.3: The distribution of x-ray AGN in redshift-SFR plane.

In the figure 4.3, we show the relationship between SFR and the number of AGN clusters correspond to redshift. where LR refers the lower redshift and HR refers high redshift; SFR1, SFR2, SFR3 and SFR4 are the SFR at different bins of our sample from -0.5 to 3.5($measured\ in\ \log(SFR)$. for example, HR_SFR4(blue) shows the distribution of x-ray AGN galaxies in the high redshift those have SFR value in range between 2.5 to 3.5(in *log (SFR)*).

Furthermore, our analysis indicates a positive correlation between the mean luminosity and SFR in both redshift regions. However, upon comparison, we observe that the higher redshift region exhibits a higher mean luminosity. This discrepancy may be attributed to various factors, such as differences in the physical conditions, evolutionary stages, or environmental properties between the low and high redshift AGN populations. Further exploration is required to ascertain the underlying reasons behind this disparity in luminosity. Lastly, we find that the stellar mass tends to be higher in the high redshift region compared to the low redshift region. This observation aligns with general expectations, as higher redshift AGN often exhibit more massive stellar components.

Additionally, our analysis indicates that in the low SFR range a higher population of AGN galaxies exist in the lower redshift region compared to the higher redshift region, this implies potential variations in the AGN demographics and evolutionary pathways across different redshifts.

The physical interpretation of our results reveals important insights into the relationship between X-ray AGN and star formation rate (SFR). The concentration of X-ray AGN in the SFR range of 1.5-2.5 suggests a favorable condition for AGN activity. This indicates that a specific range of star formation activity may play a significant role in triggering or fueling AGN. The differences in population distribution across SFR bins and redshift regions suggest varying mechanisms and conditions driving AGN activity. In the low redshift region, a higher population of AGN in the third SFR range implies distinct processes at this SFR levels. In the high redshift region, the absence of AGN in the lowest SFR bin and concentration in the third and fourth bins highlight the importance of considering star formation in AGN formation and evolution. The positive correlation between mean luminosity and SFR suggests a connection between star formation and AGN energy output, with higher redshift AGN exhibiting higher luminosity. Additionally, the higher stellar mass in the high redshift region aligns with expectations, indicating a relationship between AGN activity, star formation, and galaxy evolution.

These physical interpretations enhance our understanding of the complex interplay between AGN and star formation processes in different cosmic environments.

4.4 Comparing the AGN Galaxy Clusters with Normal Galaxy Clusters

In this section, we compare the clustering of X-ray selected AGN with that of normal galaxies. We use the 804 X-ray AGN and 2880 galaxies with available KiDS/VIKING+WISE photometry, and we construct galaxy samples that match the stellar mass, luminosity and SFR distribution of the X-ray data set. Comparing the clustering of X-ray selected AGN with that of normal galaxies is important because it can provide insights into the physical processes that drive the formation and evolution of AGN. AGN are believed to be powered by accretion onto supermassive black holes at the centers of galaxies. The properties and distribution of AGN may therefore be closely linked to the large-scale structure of their host galaxies.

By constructing galaxy samples that match the stellar mass, luminosity, and SFR distribution of the X-ray data set, we can control for potential biases and ensure that any differences in clustering are due to the presence of an AGN rather than differences in galaxy properties. If the clustering of X-ray selected AGN is found to differ significantly from that of normal galaxies, it would suggest that the presence of an AGN is affecting the large-scale structure of the host galaxy. This comparison can also provide constraints on models of AGN feedback, which is thought to play a crucial role in regulating star formation and galaxy evolution. Understanding how AGN feedback interacts with the surrounding gas and affects the distribution of matter on large scales is essential for developing a comprehensive picture of galaxy evolution.

Comparison upon Luminosity

Our finding shows that the clustering of normal galaxies and X-ray AGN shows similar dependence on galaxy properties, but with different luminosity distributions, is fascinating and provides valuable insights into the nature of AGN and their host galaxies. The AGN distribution is peak at higher luminosity while the normal galaxy distribution is peak at lower luminosity. Let's interpret this result further:

Similar dependence on galaxy properties shows the fact that both normal galaxies and X-ray AGN exhibit a similar dependence on galaxy properties in terms of clustering suggests that common underlying mechanisms may be at play. This implies that the physical processes governing the formation and evolution of galaxies, such as the growth of structures and environmental influences, are likely to have a similar impact on both normal galaxies and those hosting AGN.

Different luminosity distributions show the difference in luminosity distributions between normal galaxies and X-ray AGN indicates a distinct characteristic associated with AGN activity. The peak in AGN galaxy distribution at higher luminosities suggests that AGN tend to reside in galaxies with more intense or enhanced accretion onto supermassive black holes, resulting in higher energy outputs. This aligns with the notion that AGN are fueled by the accretion of substantial amounts of material onto the central black hole, leading to the release of enormous amounts of radiation.

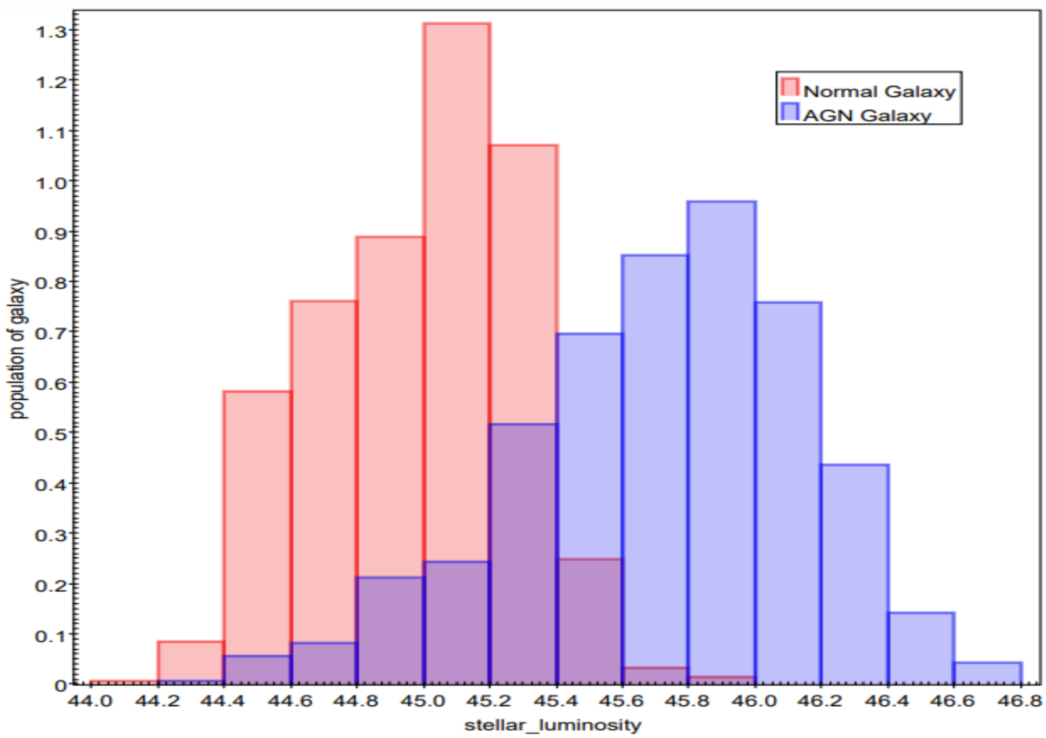

Figure 4.4: Stellar Luminosity of normalized distributions of the AGN (red) and the normal galaxies (blue).

Another key point is that AGN as a result of galaxy evolution; the higher luminosity peak in the AGN galaxy distribution suggests that AGN activity is more prevalent in galaxies with a certain level of mass or evolutionary stage.

This result supports the idea that AGN activity is a consequence of galaxy evolution, where specific conditions or stages trigger the onset of AGN. It is possible that processes such as galaxy mergers, interactions, or the build-up of mass through cosmic accretion play a role in fueling AGN and driving them to higher luminosities (Gordon, 2018).

Additionally, the difference in luminosity distributions between normal galaxies and AGN has implications for AGN feedback. AGN feedback refers to the processes through which AGN activity can influence the surrounding gas, regulate star formation, and impact the growth of the host galaxy. The higher luminosity AGN may have a more significant impact on their environment due to their increased energy output. This suggests that high-luminosity AGN could potentially have a stronger influence on quenching star formation or shaping the properties of their host galaxies through feedback processes

Totally, the finding of similar clustering dependence on galaxy properties but distinct luminosity distributions between normal galaxies and X-ray AGN provides insights into the connection between AGN activity and galaxy evolution. The higher luminosity peak in the AGN galaxy distribution indicates the prevalence of more intense AGN activity in galaxies with specific characteristics, suggesting a connection between AGN and galaxy evolution processes. Understanding this relationship is crucial for unraveling the role of AGN in shaping the properties and large-scale structure of their host galaxies.

Comparison upon stellar mass

Secondly, we present the comparison of AGN and normal galaxy based on the stellar mass of host galaxy. Our analysis reveals a fascinating pattern in the distribution of AGN and normal galaxies based on their stellar mass (see figure 4.6). It appears that the peak of AGN distribution occurs at lower stellar masses, specifically up to a logarithm of 10.3 in $M_{\odot}$ units. In contrast, the distribution of normal galaxies reaches its peak at higher stellar masses, specifically up to a logarithm of 11.3. Remarkably, despite the transition to normal galaxies, the AGN population remains more abundant than that of normal galaxies.

This finding has significant physical implications. The higher occurrence of AGN at lower stellar masses suggests that there is a connection between the growth of supermassive black holes and the early stages of galaxy formation. AGN are known to be powered by accretion onto supermassive black holes, which release tremendous amounts of energy and influence the surrounding environment this result align with the previous study which shows the energy from AGN (Pouliasis, Mountrichas, et al., 2020) . The prevalence of AGN in this lower stellar mass range suggests that the black hole growth mechanism plays a vital role in shaping the properties and evolution of galaxies during their early stages.

On the other hand, the dominance of normal galaxies at higher stellar masses indicates a transition towards a more quiescent phase of galaxy evolution. As galaxies grow and accumulate stellar mass over time, the AGN activity tends to diminish, leading to a decline in the AGN population. This shift may indicate a decline in gas supply for black hole accretion or the stabilization of the galactic environment, resulting in reduced AGN activity.

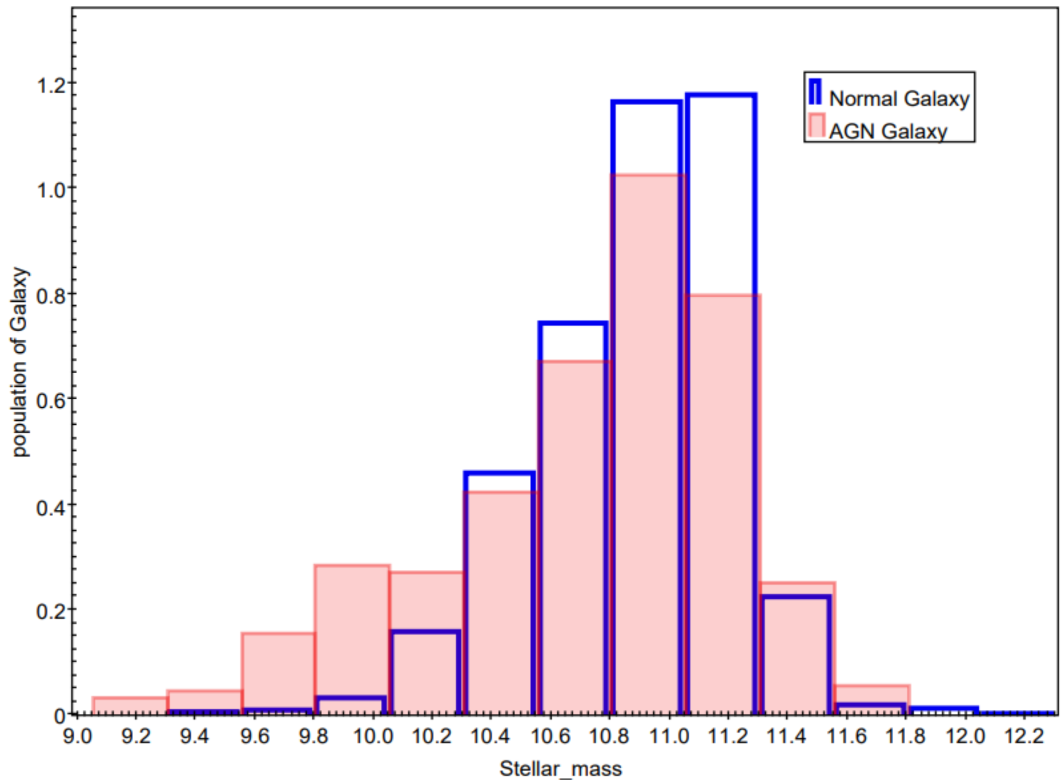

Figure 4.5: Stellar mass of normalized distributions of the AGN (red) and the normal galaxies (blue).

In summary, our findings reveal a distinct distribution of AGN and normal galaxies with respect to stellar mass. The higher prevalence of AGN at lower stellar masses suggests a link between black hole growth and early galaxy formation, while the dominance of normal galaxies at higher stellar masses indicates a transition to a more quiescent phase of galaxy evolution. this work provides valuable insights into the interplay between supermassive black holes and their host galaxies, shedding light on the mechanisms that drive galaxy growth and evolution.

Comparison upon star formation Rate

Our analysis reveals that the distribution of AGN galaxies peaks at higher star formation rates (SFR) (see figure 4.6), while the distribution of normal galaxies is higher at lower SFR. This finding suggests a critical distinction between the two populations based on their star formation activity. The physical interpretation of this result is that AGN galaxies exhibit a higher level of ongoing star formation compared to normal galaxies. AGN are known to be fueled by the accretion of material onto supermassive black holes, which releases significant amounts of energy and can influence star formation processes within galaxies. The higher occurrence of

AGN galaxies at higher SFR suggests a strong connection between AGN activity and the presence of actively forming stars.

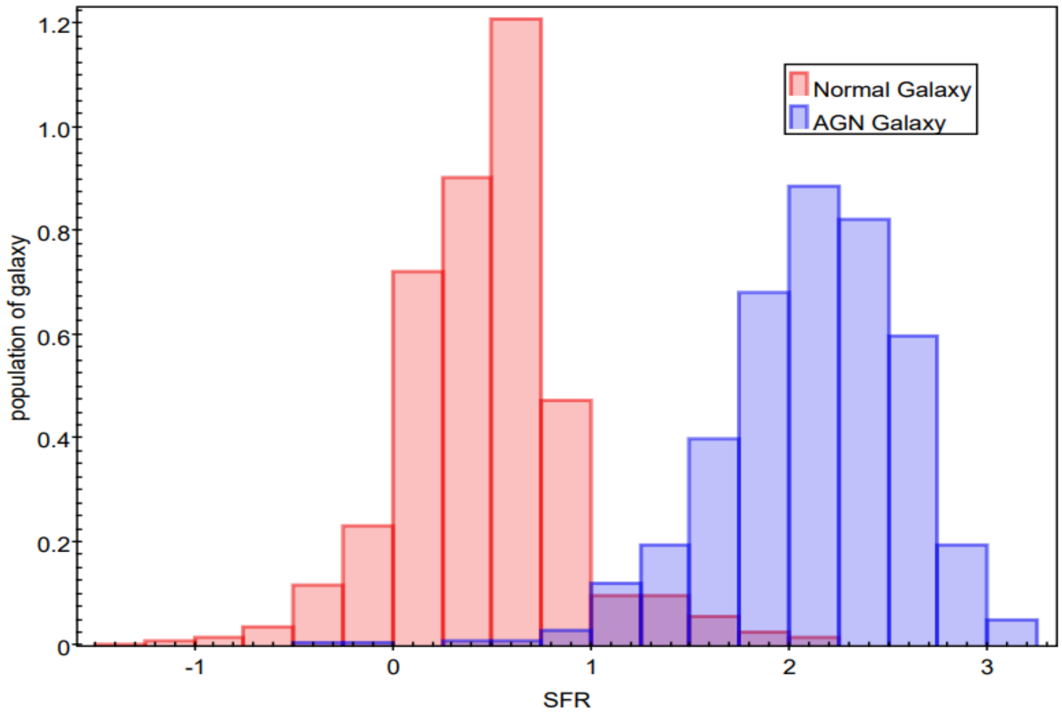

Figure 4.6: Star formation Rate (SFR) of normalized distributions of the AGN (blue) and the normal galaxies (red).

One possible explanation is that the accretion process in AGN galaxies is fueled by the availability of gas and dust, which are essential for both star formation and black hole growth. The higher SFR in AGN galaxies indicates a higher abundance of gas and dust, providing the necessary fuel for both processes to occur concurrently. The interaction between the inflowing material and the central black hole not only powers the AGN but also triggers and enhances star formation activity in the surrounding regions.

In contrast, normal galaxies show a higher prevalence at lower SFR, indicating a lower level of ongoing star formation. This could be attributed to various factors such as the depletion of gas reservoirs, a less favorable environment for star formation, or a transition to a more quiescent phase of galactic evolution. Normal galaxies may have already consumed a significant portion of their available gas or experienced a decline in the influx of fresh gas, leading to a reduced SFR.

In summary, the higher distribution of AGN galaxies at higher SFR suggests a close relationship between AGN activity and ongoing star formation. The concurrent presence of active black hole accretion and star formation processes in AGN galaxies indicates a shared fuel source, likely abundant gas and dust. On the other hand, normal galaxies exhibit a higher prevalence at lower SFR, suggesting a decrease in star formation activity, potentially due to gas depletion or a shift towards a more quiescent evolutionary phase.

CHAPTER FIVE

CONCLUSION AND RECOMMENDATION

5.1 Conclusion

In this study, we have explored the influence of host galaxy properties on X-ray AGN clusters, investigating the dependencies on luminosity, stellar mass, and star formation rate while comparing them with non-AGN clusters. By integrating multiwavelength galaxy data and utilizing the CIGALE code for SED fitting, we have obtained comprehensive insights into the correlation and relationship between AGN clusters and host galaxy properties. Our analysis revealed significant associations between luminosity, stellar mass, and star formation rate, providing valuable understanding of AGN activity. Furthermore, the comparison with non-AGN clusters uncovered distinctive characteristics, shedding light on the unique nature of AGN clusters.

In our study examining the dependence of AGN clusters on host galaxy properties, we made several key observations. First, when investigating the relationship between AGN clusters and luminosity, we found that AGN clusters exhibited significant differences in their populations across various luminosity levels. Interestingly, a large number of AGN clusters were concentrated in the middle range of luminosity $(45 < logL_{(0.5-2.0\ keV)} < 46)$ for both low and high redshift classifications. Second, with respect to the dependence of AGN clusters on stellar mass, our results indicated that galaxies hosting AGNs detected in X-ray emission tended to fall within a specific range of stellar mass, between 10 and 11 (measured in $l$og $(M_{\star}(M_{\odot})$. This range was populated by a significant proportion of AGN galaxies, regardless of their redshift classification. Finally, when examining the dependence of AGN clusters on star formation rate (SFR), we observed a significant population of X-ray AGN concentrated within the SFR range of 1.5-2.5 (expressed in $l$og $(M_{\odot} yr^{-1})$) in both the low and high redshift regions.

In our analysis, we explored various aspects of AGN clusters, including their luminosity, stellar mass, and star formation rate (SFR). Starting with luminosity, we discovered a consistent increase in mean stellar mass as luminosity increased for both low and high redshifts. This positive correlation indicates that AGN with higher luminosities tend to be hosted by galaxies with larger stellar masses. Additionally, we examined the relationship between SFR and stellar mass across different redshift regions, finding a positive correlation in both cases.

This suggests that galaxies with higher stellar masses tend to exhibit higher levels of star formation. Furthermore, our analysis revealed a positive correlation between mean luminosity and SFR in both redshift regions, emphasizing their interconnected nature.

Moving on, we compared the clustering of X-ray selected AGN with that of normal galaxies. To ensure a fair comparison, we constructed galaxy samples that matched the stellar mass, luminosity, and SFR distribution of the X-ray data set, thus controlling for potential biases and isolating the influence of AGN presence on clustering. Our findings demonstrated that both AGN and normal galaxies exhibited dependence on galaxy properties in terms of clustering, but degree of their dependance is different in different galaxy property values. The AGN distribution peaked at higher luminosity levels, while the normal galaxy distribution peaked at lower luminosity. Furthermore, we observed that the peak of the AGN distribution occurred at lower stellar masses (up to a logarithm of 10.3 in $M_{\odot}$ units), whereas the distribution of normal galaxies reached its peak at higher stellar masses (up to a logarithm of 11.3). Regarding SFR, our analysis revealed that the distribution of AGN galaxies exhibited a peak at higher SFR levels, while the distribution of normal galaxies showed a peak at lower SFR levels.

As generally, by examining the dependencies on luminosity, stellar mass, and star formation rate, this study offers valuable insights into the correlation and relationship between AGN clusters and their host galaxies. The observed significant associations between AGN luminosity, stellar mass, and star formation rate highlight the importance of these factors in AGN activity. Additionally, the comparison with non-AGN clusters provides a unique perspective on the distinctive nature of AGN clusters. The division into different redshift groups and the categorization of host galaxy properties further enhance the depth of analysis, allowing for a comprehensive evaluation of the individual effects of these properties on AGN clusters. Overall, these results bridge the existing knowledge gap and advance our understanding of the complex relationship between AGN clusters and host galaxy properties in the field of astrophysics

5.2 Recommendation

Based on the findings and significance of this study, several recommendations emerge for future research in the field of AGN clusters and host galaxy properties. Firstly, it is recommended to expand the sample size of AGN clusters to further validate the observed associations between luminosity, stellar mass, and star formation rate. This will enhance the statistical robustness of the results and provide a more comprehensive understanding of AGN activity. Additionally, future studies should explore other host galaxy properties, such as morphology, gas content, and environment, to uncover further insights into the unique nature of AGN clusters. Incorporating these additional properties will contribute to a holistic understanding of the factors influencing AGN activity.

Furthermore, it is recommended to investigate the evolutionary aspects of AGN clusters by studying their temporal variations and examining the connections between AGN activity and galaxy evolution processes. This will provide deeper insights into the co-evolution of AGNs and their host galaxies. Lastly, the utilization of advanced observational facilities and techniques, such as upcoming space missions and next-generation telescopes, should be considered to enhance the observational capabilities and resolution in studying AGN clusters and their host galaxy properties. By addressing these recommendations, future studies will further advance our understanding of AGN clusters and their relation to host galaxy properties, paving the way for more comprehensive analyses and breakthroughs in the field of astrophysics.

Research Fund Acknowledgment

This research project is funded by Adama Science and Technology University under the grant number ASTU/SM- R/762/23 Adama, Ethiopia.

REFERANCES

Alexander, P. P. D. M., Marco, R. J. A. B. De, Hickox, P. G. R. C., & Smolˇ, G. T. R. V. (2017). *Active galactic nuclei : what ' s in a name ?* https://doi.org/10.1007/s00159-017-0102-9

Amado, Z. B. (2021). *Properties and evolution of galaxies in galaxy clusters up to a redshift of z ∼ 1.0*.

Antonucci, R. (1993). Unified models for active galactic nuclei and quasars. *Annual Rev. Astron. Astrophys*, *31*, 473–521.

Beckmann, V., Barthelmy, S. D., Courvoisier, J.-L., Gehrels, N., Soldi, S., Tueller, J., & Wendt, G. (2007). *Hard X-ray Variability of AGN*.

Bernhard, E., Grimmett, L. P., Mullaney, J. R., Daddi, E., Tadhunter, C., & Jin, S. (2019). Inferring a difference in the star-forming properties of lower versus higher X-ray luminosity AGNs. *Monthly Notices of the Royal Astronomical Society: Letters*, *483*(1), L52–L57. https://doi.org/10.1093/mnrasl/sly217

Boquien, M., Burgarella, D., Roehlly, Y., Buat, V., Ciesla, L., Corre, D., Inoue, A. K., & Salas, H. (2019). CIGALE: A python Code Investigating GALaxy Emission. *Astronomy and Astrophysics*, *622*. https://doi.org/10.1051/0004-6361/201834156

Brandt, W. N., & Alexander, D. M. (2015). Cosmic X-ray surveys of distant active galaxies: The demographics, physics, and ecology of growing supermassive black holes. *Astronomy and Astrophysics Review*, *23*(1), 1–93. https://doi.org/10.1007/s00159-014-0081-z

Brunner, H., Liu, T., Lamer, G., Georgakakis, A., Merloni, A., Brusa, M., Bulbul, E., Dennerl, K., Friedrich, S., Liu, A., Maitra, C., Nandra, K., Ramos-Ceja, M. E., Sanders, J. S., Stewart, I. M., Boller, T., Buchner, J., Clerc, N., Comparat, J., … Wilms, J. (2022). The eROSITA Final Equatorial Depth Survey (eFEDS): X-ray catalogue. *Astronomy and Astrophysics*, *661*. https://doi.org/10.1051/0004-6361/202141266

Cappelluti, N., Ajello, M., Burlon, D., Krumpe, M., Miyaji, T., Bonoli, S., & Greiner, J. (2010). Active galactic nuclei clustering in the local universe: An unbiased picture from swift-bat. *Astrophysical Journal Letters*, *716*(2), L209–L213.

https://doi.org/10.1088/2041-8205/716/2/L209

Clarke, A. O., Heald, G., Jarrett, T., Bray, J. D., Hardcastle, M. J., Cantwell, T. M., Scaife, A. M. M., Brienza, M., Bonafede, A., Breton, R. P., Broderick, J. W., Carbone, D., Croston, J. H., Farnes, J. S., Harwood, J. J., Heesen, V., Horneffer, A., Van Der Horst, A. J., Iacobelli, M., … Wise, M. W. (2017). LOFAR MSSS: Discovery of a 2.56 Mpc giant radio galaxy associated with a disturbed galaxy group. *Astronomy and Astrophysics*, *601*, 1–9. https://doi.org/10.1051/0004-6361/201630152

Coil, A. L., Georgakakis, A., Newman, J. A., Cooper, M. C., Croton, D., Davis, M., Koo, D. C., Laird, E. S., Nandra, K., Weiner, B. J., Willmer, C. N. A., & Yan, R. (2009). Aegis: The clustering of x-ray active galactic nucleus relative to galaxies at z 1. *Astrophysical Journal*, *701*(2), 1484–1499. https://doi.org/10.1088/0004-637X/701/2/1484

Crossett, J. P., Pimbblet, K. A., Jones, D. H., Brown, M. J. I., & Stott, J. P. (2017). *Near-ultraviolet signatures of environment-driven galaxy quenching in Sloan Digital Sky Survey groups 1 I N T RO D U C T I O N*. *490*, 480–490. https://doi.org/10.1093/mnras/stw2228

Curtis, H. D., Curtis, & D., H. (1918). Descriptions of 762 Nebulae and Clusters Photographed with the Crossley Reflector. *PLicO*, *13*, 9–42. https://ui.adsabs.harvard.edu/abs/1918PLicO..13....9C/abstract

Davies, L. J. M., Huynh, M. T., Hopkins, A. M., Seymour, N., Driver, S. P., Robotham, A. G. R., Baldry, I. K., Bourne, N., Bremer, M. N., Brown, M. J. I., Brough, S., Cluver, M., Grootes, M. W., Jarvis, M., Loveday, J., Moffet, A., Owers, M., Phillipps, S., Sadler, E., … Wright, A. (2017). *Galaxy And Mass Assembly : the 1 . 4 GHz SFR indicator , SFR – M ∗ relation and predictions for ASKAP – GAMA 1 I N T RO D U C T I O N*. *2324*, 2312–2324. https://doi.org/10.1093/mnras/stw3080

Davis, S. W., & Laor, A. (2011). The radiative efficiency of accretion flows in individual active galactic nuclei. *Astrophysical Journal*, *728*(2). https://doi.org/10.1088/0004-637X/728/2/98

Delvecchio, I., Gruppioni, C., Pozzi, F., Berta, S., Zamorani, G., Cimatti, A., Lutz, D., Scott, D., Vignali, C., Cresci, G., Feltre, A., Cooray, A., Vaccari, M., Fritz, J., Le Floc'h, E., Magnelli, B., Popesso, P., Oliver, S., Bock, J., … Scodeggio, M. (2014). Tracing the cosmic growth of supermassive black holes to z ~3 with Herschel. *Monthly Notices of the*

Royal Astronomical Society, *439*(3), 2736–2754. https://doi.org/10.1093/mnras/stu130

Denis, B., Mederic, B., Veronique, B., Laure, C., & Yannick, R. (2017). Galaxy Sed Fitting. *Publications of The Korean Astronomical Society*, *32*(1), 205–208. https://doi.org/10.5303/pkas.2017.32.1.205

Dickinson, M., Papovich, C., Ferguson, H. C., & Budavari, T. (2003). The Evolution of the Global Stellar Mass Density at 0 < z < 3 . *The Astrophysical Journal*, *587*(1), 25–40. https://doi.org/10.1086/368111

Ebeling, H., Stephenson, L. N., & Edge, A. C. (2014). *JELLYFISH : EVIDENCE OF EXTREME RAM-PRESSURE STRIPPING IN MASSIVE GALAXY CLUSTERS ∗*. *40*, 2006–2010. https://doi.org/10.1088/2041-8205/781/2/L40

Edge, D. O., Shakeshaft, J. R., McAdam, W. B., Baldwin, J. E., Archer, S., Edge, D. O., Shakeshaft, J. R., McAdam, W. B., Baldwin, J. E., & Archer, S. (1959). A survey of radio sources at a frequency of 159 Mc/s. *MmRAS*, *68*, 37–60. https://ui.adsabs.harvard.edu/abs/1959MmRAS..68...37E/abstract

Ellison, S. L., Patton, D. R., Simard, L., Mcconnachie, A. W., Baldry, I. K., & Mendel, J. T. (2010). *Galaxy pairs in the Sloan Digital Sky Survey – II . The effect of environment on interactions 1 I N T RO D U C T I O N*. *1528*, 1514–1528. https://doi.org/10.1111/j.1365-2966.2010.17076.x

Falco, M., Hansen, S. H., Wojtak, R., Brinckmann, T., Lindholmer, M., & Pandolfi, S. (2014). A new method to measure the mass of galaxy clusters. *Monthly Notices of the Royal Astronomical Society*, *442*(2), 1887–1896. https://doi.org/10.1093/MNRAS/STU971

Fanidakis, N., Georgakakis, A., Mountrichas, G., Krumpe, M., Baugh, C. M., Lacey, C. G., Frenk, C. S., Miyaji, T., & Benson, A. J. (2013). Constraints on black hole fuelling modes from the clustering of X-ray AGN. *Monthly Notices of the Royal Astronomical Society*, *435*(1), 679–688. https://doi.org/10.1093/mnras/stt1327

Fath, E. A., Fath, & Arthur, E. (1909). The spectra of some spiral nebulae and globular star clusters. *LicOB*, *149*(2064), 71–77. https://doi.org/10.5479/ADS/BIB/1909LICOB.5.71F

Giacconi, R., Murray, S., Gursky, H., Kellogg, E., Schreier, E., Matilsky, T., D. Koch, A., & Tananbaum, H. (1974). THE THIRD UHURU CATALOG OF X-RAY SOURCES. *The American Astronomical Society*.

Gordon, Y. A. (2018). Observing the Effect of Galaxy Environment on the Evolution of

Active Galactic Nuclei in the Era of Multiplexed Wide-Field Fibre-Optic Spectroscopy. *Department of Physics*, *The University of Hull*, *February*. http://adsabs.harvard.edu/abs/2018PhDT........60G

Hönig, S. F. (2019). Redefining the Torus: A Unifying View of AGNs in the Infrared and Submillimeter. *The Astrophysical Journal*, *884*(2), 171. https://doi.org/10.3847/1538-4357/ab4591

Ishibashi, W., Auger, M. W., Zhang, D., & Fabian, A. C. (2014). Radio-mode feedback in local AGNs: Dependence on the central black hole parameters. *Monthly Notices of the Royal Astronomical Society*, *443*(2), 1339–1345. https://doi.org/10.1093/mnras/stu1236

Kamraj, N. (2022). *Probing the Corona in Active Galactic Nuclei Using Broadband X-ray Spectroscopy Thesis by*. *September 2021*.

Kleiner, D., Pimbblet, K. A., Jones, D. H., Koribalski, S., & Serra, P. (2021). *Evidence for H i replenishment in massive galaxies through gas accretion from the cosmic web*. *19*(June), 1–19.

Koutoulidis, L., Mountrichas, G., Georgantopoulos, I., Pouliasis, E., & Plionis, M. (2022). Host galaxy properties of X-ray active galactic nuclei in the local Universe. *Astronomy and Astrophysics*, *658*(42466), 2–9. https://doi.org/10.1051/0004-6361/202142466

Koutoulidis, L., Plionis, M., Georgantopoulos, I., & Fanidakis, N. (2013). Clustering, bias and the accretion mode of X-ray-selected AGN. *Monthly Notices of the Royal Astronomical Society*, *428*(2), 1382–1394. https://doi.org/10.1093/mnras/sts119

Krolik, J. H. (1999). Magnetized Accretion inside the Marginally Stable Orbit around a Black Hole. *The Astrophysical Journal*, *515*(2), L73–L76. https://doi.org/10.1086/311979

Krumpe, M., Miyaji, T., Coil, A. L., & Aceves, H. (2012). The spatial clustering of ROSAT All-Sky Survey active galactic nuclei. III. Expanded sample and comparison with optical active galactic nuclei. *Astrophysical Journal*, *746*(1). https://doi.org/10.1088/0004-637X/746/1/1

Krumpe, M., Miyaji, T., Husemann, B., Fanidakis, N., Coil, A. L., & Aceves, H. (2015). THE SPATIAL CLUSTERING of ROSAT ALL-SKY SURVEY ACTIVE GALACTIC NUCLEI. IV. MORE MASSIVE BLACK HOLES RESIDE in MORE MASSIVE DARK MATTER HALOS. *Astrophysical Journal*, *815*(1), 21. https://doi.org/10.1088/0004-637X/815/1/21

Kuijken, K., Heymans, C., Dvornik, A., Hildebrandt, H., De Jong, J. T. A., Wright, A. H., Erben, T., Bilicki, M., Giblin, B., Shan, H. Y., Getman, F., Grado, A., Hoekstra, H., Miller, L., Napolitano, N., Paolilo, M., Radovich, M., Schneider, P., Sutherland, W., … Verdoes Kleijn, G. A. (2019). The fourth data release of the Kilo-Degree Survey: Ugri imaging and nine-band optical-IR photometry over 1000 square degrees. *Astronomy and Astrophysics*, *625*(October 2011), 1–25. https://doi.org/10.1051/0004-6361/201834918

Lang, K. R. (2013). *Undergraduate Lecture Notes in Physics: Essential Astrophysics*.

Leslie, S. K., Kewley, L. J., Sanders, D. B., & Lee, N. (2016). Quenching star formation: Insights from the local main sequence. *Monthly Notices of the Royal Astronomical Society*, *455*(1), L82–L86. https://doi.org/10.1093/mnrasl/slv135

Masoura, V. A., Mountrichas, G., Georgantopoulos, I., & Plionis, M. (2021). Relation between AGN type and host galaxy properties. *Astronomy and Astrophysics*, *646*, 1–11. https://doi.org/10.1051/0004-6361/202039238

Masoura, V. A., Mountrichas, G., Georgantopoulos, I., Ruiz, A., Magdis, G., & Plionis, M. (2018). Disentangling the AGN and star formation connection using XMM-Newton. *Astronomy and Astrophysics*, *618*, 1–9. https://doi.org/10.1051/0004-6361/201833397

Masters, K. L., Mosleh, M., Romer, A. K., Nichol, R. C., Bamford, S. P., Schawinski, K., Lintott, C. J., Andreescu, D., Campbell, H. C., Crowcroft, B., Doyle, I., Edmondson, E. M., Murray, P., Raddick, M. J., Szalay, A. S., & Vandenberg, J. (2018). *Galaxy Zoo : Passive Red Spirals* ∗. *20*(October), 1–20.

Merritt, D., & Ferrarese, L. (2001). The M • -σ Relation for Supermassive Black Holes . *The Astrophysical Journal*, *547*(1), 140–145. https://doi.org/10.1086/318372

Mountrichas, G., Georgakakis, A., & Georgantopoulos, I. (2019). The dependence of the X-ray AGN clustering on the properties of the host galaxy. *Monthly Notices of the Royal Astronomical Society*, *483*(1), 1374–1387. https://doi.org/10.1093/mnras/sty3140

Mountrichas, G., Georgakakis, A., Menzel, M. L., Fanidakis, N., Merloni, A., Liu, Z., Salvato, M., & Nandra, K. (2016). The clustering amplitude of X-ray-selected AGN at z ~ 0.8: Evidence for a negative dependence on accretion luminosity. *Monthly Notices of the Royal Astronomical Society*, *457*(4), 4195–4204. https://doi.org/10.1093/mnras/stw281

Mountrichas, G., & Shankar, F. (2022). Testing the evolutionary pathways of galaxies and their supermassive black holes and the impact of feedback from Active Galactic Nuclei via large multiwavelength datasets. *Monthly Notices of the Royal Astronomical Society*, *November*. https://doi.org/10.1093/mnras/stac3211

Pan, C., Vogeley, M. S., Hoyle, F., Choi, Y., & Park, C. (2018). *Cosmic Voids in Sloan Digital Sky Survey Data Release 7*. *000*(August).

Pandey, D., Saha, K., Pradhan, A. C., & Kaviraj, S. (2022). *Central star formation in an early-type galaxy I Zw 81 in the Bootes void*.

Pitk, M. (2020). *A Model for the Formation of Galaxies*. *11*(2), 90–99.

Pouliasis, E., Georgantopoulos, I., Bonanos, A. Z., Yang, M., Sokolovsky, K. V., Hatzidimitriou, D., Mountrichas, G., Gavras, P., Charmandaris, V., Bellas-Velidis, I., Spetsieri, Z. T., & Tsinganos, K. (2019). Robust identification of active galactic nuclei through HST optical variability in GOODS-S: Comparison with the X-ray and mid-IR-selected samples. *Monthly Notices of the Royal Astronomical Society*, *487*(3), 4285–4304. https://doi.org/10.1093/mnras/stz1483

Pouliasis, E., Georgantopoulos, I., Ruiz, A., Gilli, R., Koulouridis, E., Akiyama, M., Ueda, Y., Chiappetti, L., Garrel, C., Horellou, C., Nagao, T., Paltani, S., Pierre, M., Toba, Y., & Vignali, C. (2022). XXL-HSC: An updated catalogue of high-redshift (z3.5) X-ray AGN in the XMM-XXL northern field: Constraints on the bright end of the soft log N -log S. *Astronomy and Astrophysics*, *658*. https://doi.org/10.1051/0004-6361/202142059

Pouliasis, E., Mountrichas, G., Georgantopoulos, I., Ruiz, A., Yang, M., & Bonanos, A. Z. (2020). An obscured AGN population hidden in the VIPERS galaxies: Identification through spectral energy distribution decomposition. *Monthly Notices of the Royal Astronomical Society*, *495*(2), 1853–1873. https://doi.org/10.1093/mnras/staa1263

Pouliasis, E., Pouliasis, & Ektoras. (2020). Identification of Active Galactic Nuclei through different selection techniques. *PhDT*. https://ui.adsabs.harvard.edu/abs/2020PhDT.........3P/abstract

Predehl, P., Andritschke, R., Arefiev, V., Babyshkin, V., Batanov, O., Becker, W., Böhringer, H., Bogomolov, A., Boller, T., Borm, K., Bornemann, W., Bräuninger, H., Brüggen, M., Brunner, H., Brusa, M., Bulbul, E., Buntov, M., Burwitz, V., Burkert, W., … Yaroshenko, V. (2021). The eROSITA X-ray telescope on SRG. *Astronomy and Astrophysics*, *647*. https://doi.org/10.1051/0004-6361/202039313

Ragavan, D. (2021). Multiwavelength observations of Galaxy Clusters. *Academia Letters*, *June*, 0–10. https://doi.org/10.20935/al1213

Revalski, M., Meena, B., Martinez, F., Polack, G. E., Crenshaw, D. M., Kraemer, S. B., Collins, N. R., Fischer, T. C., Schmitt, H. R., Schmidt, J., Maksym, W. P., & Rafelski, M. (2021). Quantifying Feedback from Narrow Line Region Outflows in Nearby Active Galaxies. III. Results for the Seyfert 2 Galaxies Markarian 3, Markarian 78, and NGC 1068* † . *The Astrophysical Journal*, *910*(2), 139. https://doi.org/10.3847/1538-4357/abdcad

Robotham, A. S. G., Norberg, P., Driver, S. P., Baldry, I. K., Bamford, S. P., Hopkins, A. M., Liske, J., Loveday, J., Merson, A., Peacock, J. A., Brough, S., Cameron, E., Conselice, C. J., Croom, S. M., Frenk, C. S., Gunawardhana, M., Hill, D. T., Jones, D. H., Kelvin, L. S., … Wijesinghe, D. (2011). *Galaxy and Mass Assembly (GAMA): the GAMA galaxy group catalogue (G 3 Cv1) 1 I N T RO D U C T I O N*. *2668*, 2640–2668. https://doi.org/10.1111/j.1365-2966.2011.19217.x

Rosati, P., Borgani, S., Norman, C., European, E. S. O., Observatory, S., & M, D.-G. (2002). *The Evolution of X-ray Clusters of Galaxies*. 539–577.

Salvato, M., Wolf, J., Dwelly, T., Georgakakis, A., Brusa, M., Merloni, A., Liu, T., Toba, Y., Nandra, K., Lamer, G., Buchner, J., Schneider, C., Freund, S., Rau, A., Schwope, A., Nishizawa, A., Klein, M., Arcodia, R., Comparat, J., … Nitschelm, C. (2022). The eROSITA Final Equatorial-Depth Survey (eFEDS): Identification and characterization of the counterparts to point-like sources. *Astronomy and Astrophysics*, *661*, 1–32. https://doi.org/10.1051/0004-6361/202141631

Scudder, J. M., Ellison, S. L., & Mendel, J. T. (2012). *The dependence of galaxy group star formation rates and metallicities on large-scale environment 1 I N T RO D U C T I O N*. *2704*, 2690–2704. https://doi.org/10.1111/j.1365-2966.2012.21080.x

Shimizu, T. T., Mushotzky, R. F., Meléndez, M., Koss, M. J., Barger, A. J., & Cowie, L. L. (2017). Herschel far-infrared photometry of the Swift Burst Alert Telescope active galactic nuclei sample of the local universe - III. Global star-forming properties and the lack of a connection to nuclear activity. *Monthly Notices of the Royal Astronomical Society*, *466*(3), 3161–3183. https://doi.org/10.1093/mnras/stw3268

Slipher, V. M., Slipher, & M., V. (1917). The spectrum and velocity of the nebula N.G.C. 1068 (M 77). *LowOB*, *3*, 59–62.

https://ui.adsabs.harvard.edu/abs/1917LowOB...3...59S/abstract

Stalevski, M., Ricci, C., Ueda, Y., Lira, P., Fritz, J., & Baes, M. (2016). The dust covering factor in active galactic nuclei. *Monthly Notices of the Royal Astronomical Society*, *458*(3), 2288–2302. https://doi.org/10.1093/mnras/stw444

Thomas, D., Maraston, C., & Bender, R. (2004). *The epochs of early-type galaxy formation as a function of environment*.

Wilson, A. S., & Colbert, E. J. M. (1995). The difference between radio-loud and radio-quiet active galaxies. *The Astrophysical Journal*, *438*, 62. https://doi.org/10.1086/175054

Wright, E. L., Eisenhardt, P. R. M., Mainzer, A. K., Ressler, M. E., Cutri, R. M., Jarrett, T., Kirkpatrick, J. D., Padgett, D., McMillan, R. S., Skrutskie, M., Stanford, S. A., Cohen, M., Walker, R. G., Mather, J. C., Leisawitz, D., Gautier, T. N., McLean, I., Benford, D., Lonsdale, C. J., … Tsai, C. W. (2010). The Wide-field Infrared Survey Explorer (wise): Mission description and initial on-orbit performance. *Astronomical Journal*, *140*(6), 1868–1881. https://doi.org/10.1088/0004-6256/140/6/1868

Yang, G., Boquien, M., Brandt, W. N., Buat, V., Burgarella, D., Ciesla, L., Lehmer, B. D., Małek, K., Mountrichas, G., Papovich, C., Pons, E., Stalevski, M., Theulé, P., & Zhu, S. (2022). Fitting AGN/Galaxy X-Ray-to-radio SEDs with CIGALE and Improvement of the Code. *The Astrophysical Journal*, *927*(2), 192. https://doi.org/10.3847/1538-4357/ac4971

Yang, G., Brandt, W. N., Alexander, D. M., Chen, C. T. J., Ni, Q., Vito, F., & Zhu, F. F. (2019). Evident black hole-bulge coevolution in the distant universe. *Monthly Notices of the Royal Astronomical Society*, *485*(3), 3721–3737. https://doi.org/10.1093/mnras/stz611

Zou, F., Yang, G., Brandt, W. N., & Xue, Y. (2019). The Host-galaxy Properties of Type 1 versus Type 2 Active Galactic Nuclei. *The Astrophysical Journal*, *878*(1), 11. https://doi.org/10.3847/1538-4357/ab1eb1

Zubovas, K., & King, A. (2013). Bal qsos and extreme Ufos: The eddington connection. *Astrophysical Journal*, *769*(1). https://doi.org/10.1088/0004-637X/769/1/51